**ORIGINAL RESEARCH** **Open access**

# A Level-Based Coupled Optimization Method for Distributed Scheduling of Multi-Energy Systems with Renewable Energy and Electric Vehicles

Tobias Weber[1*], Hanna Müller[1]

## Abstract

Systems that synergize high-penetration, large-scale plug-in electric vehicles, distributed renewable generation, and battery energy storage hold significant promise for diminishing the power grid's dependence on conventional fossil-based fuels. Yet, the unpredictable charging mannerisms of plug-in electric vehicles, coupled with the stochastic nature of photovoltaic output, risk placing extra strain on the grid and undermining the supply–demand balance. A potent strategy to mitigate this lies in well-designed scheduling optimization. This work constructs an original scheduling framework for a Multi-energy synergy system, explicitly factoring in the controlled charging and discharging of plug-in electric vehicles and the intermittent behavior of photovoltaics, to counter problems of grid instability and unreliability. The result is a large-scale mixed-integer formulation that demands a capable and efficient solving technique. To tackle this nonlinear, large-scale, and tightly coupled unit commitment challenge, a novel binary level-based learning optimization algorithm is introduced. The practicality of the developed framework was investigated through numerical simulations spanning various unit fleet sizes and different operational scenarios. The findings conclusively demonstrate the framework's logic and efficacy for unit commitment resolutions, delivering a 3.3% decrease in costs and showcasing premier performance in large-scale energy optimization. The coordinated use of plug-in electric vehicles, distributed renewable energy generation, and battery energy storage systems is validated to reduce output from 192.72 MW units during peak demand windows, thus strengthening grid stability. Consequently, optimized energy utilization and allocation will become a vital element of future power infrastructure.

**Keywords** Renewable energy, Electric vehicle, Unit commitment, Battery energy storage system, Synergy optimization

*Correspondence:
Tobias Weber
tobias.weber@gmail.com
[1] Department of AI and Digital Energy Systems, Faculty of Engineering, University of Stuttgart, Stuttgart, Germany

## Introduction

The overriding direction within the energy domain for lowering carbon output has been the international pivot toward multi-energy decarbonization, a process in which renewable sources supplant older methods of electricity production [1]. Given the uneven spread of energy resources [2], heavyweight nations like China lean greatly on coal-burning plants for their heating and electricity needs [3]. The Multi-Energy Synergy System (MESS) weaves together plug-in electric vehicles (PEV) [4], distributed renewable energy generations (DRGs) [5] like solar PV, and battery energy storage systems (BESS) [6] with traditional thermal power stations. This cohesive architecture blends disparate energy vectors, harnessing intelligent optimization tools to proficiently govern the flows of energy transmission, storage, generation, and usage [7], thereby encouraging collaborative functionality between the system's constituent parts. Setting it apart from

This is an open access article distributed under the terms of the Creative Commons Attribution-NonCommercial-ShareAlike 4.0 International License (CC BY-NC-SA 4.0), which permits non-commercial use, distribution, reproduction, and adaptation in any medium or format, provided that appropriate credit is given to the original author(s) and source, a link to the license is provided, and any changes made are indicated. Adapted material must be distributed under the same license.

© 2023 The Author(s). | Published by Institute of Smart Energy Systems Press

Integrated Energy Systems (IES), the MESS concept emphasizes deeper reciprocal interactions and synergies across various energy types. A hallmark of the MESS design is its heightened agility, allowing it to nimbly and proactively respond to shifts in power consumption and generation. Such responsiveness is critical for successfully navigating the fluctuations and peak-demand challenges tied to DRGs.

The broad integration of varied energy sources within the MESS paradigm introduces a formidable problem of sharp energy volatility, a condition that can trigger grid instability. The generating assets within the MESS are thus forced into repetitive cycling on and off to preserve energy balance, a dynamic that intensifies the economic penalties [8], a situation widely recognized as the unit commitment (UC) dilemma. At present, the separate integration and intelligent orchestration of PEV, DRG, and BESS modules have become a practical pathway for confronting UC problems. First, the PEV submodule within the MESS structure can reduce grid strain by avoiding overload conditions during peak consumption hours [9] through smart coordination of its charge/discharge cycles [10]. Reference [11] presented a constrained optimization method aimed at achieving cost-sensitive battery charging from the perspective of PEV owners. Next, the inclusion of DRGs in the MESS framework [12], notably photovoltaics [13], helps relieve pressure on the electrical infrastructure [14]. A stochastic programming-based scheduling model was proposed in Ref. [15] to reduce solar PV forecast inaccuracy, thereby improving voltage stability on the grid. That said, today's typical systems still depend on non-renewable [16] spinning reserves to guarantee a steady on-demand supply and throttle back production when there is surplus energy [17]. The coordinated and uncoordinated charging setups for grid-linked EVs alongside photovoltaic systems were addressed in Refs. [18] and [19] using traditional combinatorial optimization methods. Third, similar to DRGs and PEVs, incorporating coordinated BESS into MESS yields numerous advantages for the grid [20], including operational expense reductions [21], voltage stabilization [22], and functioning as a grid reserve [23]. The application of BESS in MESS configurations has proven to be a highly efficient strategy for the reliable, dependable, and instantaneous operation of modern grids [24]. A distributed battery architecture was proposed in Ref. [25] to reduce the required battery capacities through optimized excess-energy pooling and shared storage resources.

The foundation established by the investigations mentioned above is at the leading edge. The mutual dependencies among DRGs, PEVs, and BESS within a MESS form a unified energy environment that boosts the exploitation of renewable assets while making the grid more flexible and robust. Nevertheless, given the intermittent output typical of most DRGs, PV output is heavily influenced by meteorological factors [26], and the power system's volatility is projected to become increasingly pronounced as DRGs claim an ever-larger share of the supply portfolio [27]. Beyond that, the upfront capital needed for BESS is markedly steep, and various BESS configurations incur significant ongoing upkeep costs [28]. Concurrently, the erratic recharging profiles of a massive PEV fleet pose deep-seated risks to grid dependability [29] and its secure operation [30]. As electric vehicles and DRGs undergo widespread proliferation and integration [31], the associated data intricacy grows, making greater inter-module coupling within the MESS an imperative.

When power grid infrastructures are designed to accommodate only one of PEVs, DRGs, or BESS in isolation, the underlying scheduling challenge takes the form of a canonical nonlinear mixed-integer optimization task. The established solution techniques for this category of scheduling problems fall broadly into two camps: analytical mathematical formulations and meta-heuristic algorithms (MAs). Among the frequently utilized mathematical tools are stochastic mixed-integer programming [32], parallel dual dynamic integer programming [33], Lagrange relaxation [34], and Quantum Surrogate Lagrangian Relaxation (QSLR) [35], all of which lend themselves well to deployment on low-dimensional UC formulations. Standing apart from these analytical routes, popular MA methodologies encompass genetic algorithm (GA) [36], differential evolution (DE) [37], ant colony optimization (ACO) [38], particle swarm optimization (PSO) [39], firefly algorithm [40], and teaching-learning-based optimization (TLBO) [41]. Thanks to their flexible encoding frameworks and often superior search processes, MAs can extract better-quality solutions when faced with UC optimization challenges. Building on this, a variety of binary-encoded MA offshoots have been proposed to address the binary conversion aspect of UC, where the state variable dictating a generator's on/off status is inherently binary. Techniques such as binary differential evolution (BDE) [42], binary particle swarm optimization (BPSO) [8], binary whale optimization algorithm (BWOA) [43], binary fish migration optimization [44], and binary artificial bee colony (DisABC) [45] all rely on transfer

© 2023 The Author(s). | Published by Institute of Smart Energy Systems Press

functions to translate continuous search spaces into binary decisions. In a different vein, quantum-inspired particle swarm optimization (QPSO) [46] and quantum-based sine cosine algorithm (Q-SCA) [47] weave in quantum computing concepts to sharpen search potency, alongside certain blended binary coding strategies like the mixed-variable variant of PSO [48] and others. Using numerical base conversion, binary MA methods can effectively manage mixed-integer programs, signaling strong promise for tackling large-scale MESS assimilation. With growing system intricacy, several fresh learning mechanisms tailored for PSO have emerged to boost overall performance. These encompass the competitive learning strategy [49], mutation-PSO [50], and the social learning strategy [51], each motivated by competitive dynamics and learning behaviors evident in human collectives. The tricompetition mechanism [52] was incorporated into CSO to lessen solution sparsity around optima. In subsequent developments, BCSO [53] and BSLPSO [54] leveraged a mechanism through which the elite particles within the current swarm steer the positional updates of the remainder, thereby enriching population diversity. Because MESS optimization involves deep coupling among assorted energy streams, it morphs into a high-dimensional, tightly interwoven mixed-integer optimization problem. A multispace evolutionary search was advanced in Ref. [55] to partition the large-scale problem into a collection of more manageable subproblems. Meanwhile, a heuristic built upon fast-forward selection was crafted in Ref. [56] to assist in the decomposition of expansive problem instances. In contrast to BCSO and BSLPSO, where merely a single superior particle's location informs the updates for the rest of the swarm during each cycle, the level-based learning swarm optimizer (LLSO) [57] sorts particles into distinct tiers and permits each particle within a given tier to refine its position by consulting two higher-performing particles selected at random from superior tiers. This arrangement not only fosters greater diversity but also calibrates the trade-off between broad exploration and focused exploitation.

Building on the investigations discussed above, the present paper introduces a multi-energy synergy optimization framework designed to reduce the generation costs of system constituents, the cycling costs of thermal units, and the charges associated with $CO_2$ emissions. The level-based learning paradigm is deployed within the MESS optimization design to assess the repercussions of embedding BESS and PV as distributed generations (DGs), along with the charge/discharge scheduling of extensive PEV fleets within the power network. Additionally, this paper formulates a binary level-based learning swarm optimization algorithm to directly confront the encoding difficulties posed by binary decision variables in EMS optimization. Toward this aim, three separate operational scenarios are executed to substantiate the practicality and soundness of the proposed MESS scheduling construct. To the best of the authors' awareness, this MESS is the inaugural system advanced to grapple with high-dimensional combinatorial optimization problems. The principal contributions delivered by this research are spotlighted below:

© 2023 The Author(s). | Published by Institute of Smart Energy Systems Press

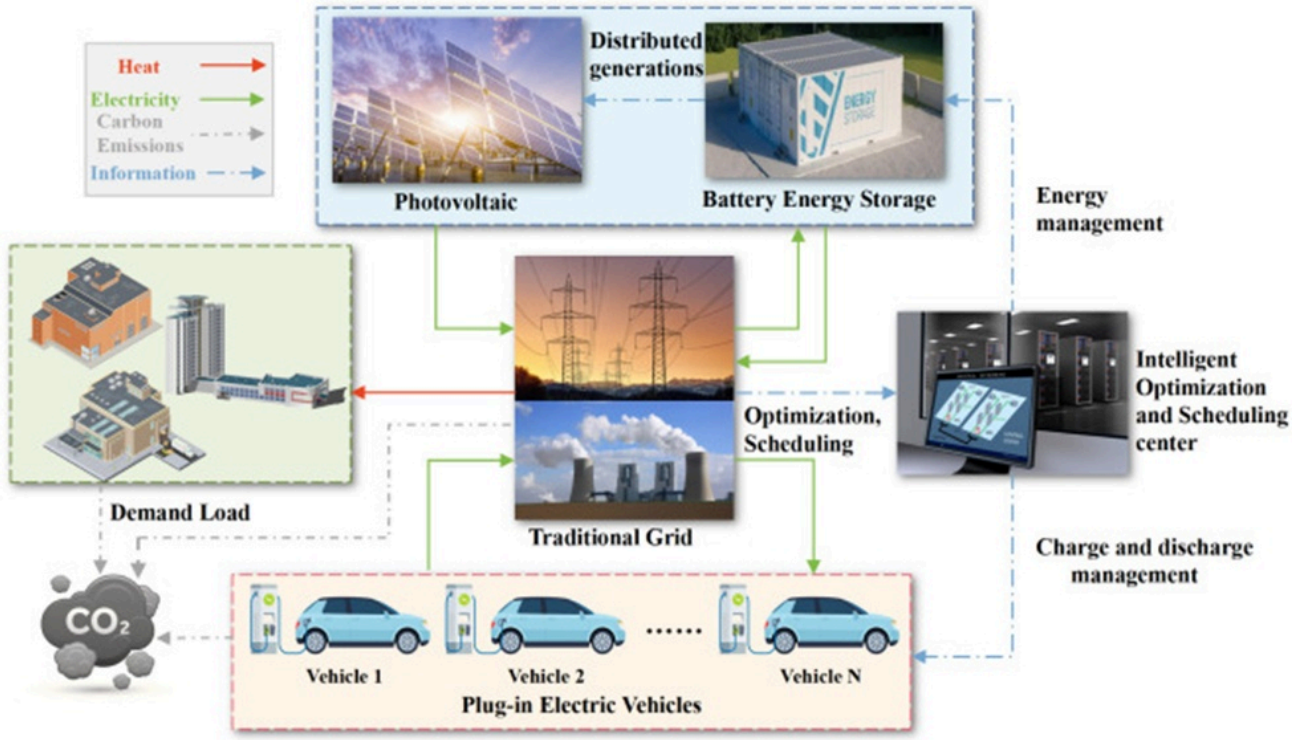


**Figure 1.** Architecture of MESSs.

• A thoroughly fused MESS scheduling framework is established for the first time, extending the scope from a lone energy source to a cohesive multi-energy amalgamation of PEVs, DRGs, and BESS, while incorporating dynamic, real-time multi-energy governance and optimization.

• A high-coupling, nonlinear mathematical model is composed to jointly minimize electricity production outlays and carbon release penalties, subject to both network-wide restrictions and unit-specific operational limits.

• An original binary level-based learning swarm algorithm is devised to sidestep the curse of dimensionality and the pitfalls of binary variable translation when solving the expansive MESS optimization formulation, by actively promoting heterogeneity across the population.

# Problem Formulation

This section opens with a depiction of the envisioned MESSs architecture. To reduce the operational expenditures of thermal units and abate carbon emissions, the objective function in this study bundles together fossil fuel outlays and the expenses stemming from carbon emissions. At the same time, a suite of essential constraints must be honored to assure safe operation, such as the power balance requirement, restrictions governing PEVs, and the upper state of charge (SoC) limits imposed on batteries, among others. Beyond this, owing to the inherent unpredictability involved, the connection of PEVs and DGs will perturb the stability of the power grid. Hence, the restrictions specific to these entities and their knock-on effects on the legacy grid must both be woven into the model.

## Description of MESS

The layout of the proposed MESSs is visualized in **Figure 1**, which brings together photovoltaic panels, thermal generating units, battery energy storage, a sizeable fleet of PEVs, and consumption loads. The PV modules capture solar irradiance and transform it into electric current, feeding it into the grid as part of the generation mix. The BESS can

© 2023 The Author(s). | Published by Institute of Smart Energy Systems Press

discharge the surplus charge accumulated throughout sunlit hours to help meet peak demand intervals when photovoltaic output dips. Furthermore, PEVs are fitted with rechargeable battery packs that can accept and hold electric charge. These vehicle batteries can be interfaced with the grid to either inject or extract power as the prevailing conditions dictate. This bi-directional flow of energy enables PEVs to act as movable storage assets, providing flexible energy support.

The MESS is tasked with continuously reconciling energy inflows (sourced from PV, thermal units, and PEVs) against outflows (stemming from varied consumption loads). For example, when PV yields an energy surplus, the extra power can be allocated to top up the PEVs, contribute to thermal storage, or be conserved in stationary batteries for future retrieval. On the flip side, during episodes of heightened consumption, the system can call upon the stored energy housed in the batteries to satisfy the load. This instantaneous, adaptive choreography among the modules is indispensable for a smoothly functioning multi-energy platform. Thus, MESSs call for the harmonization, fine-tuning, and administration of multiple modules marked by divergent traits, behavioral dynamics, and operational needs, while simultaneously navigating a host of exogenous factors and boundaries.

## Objective function

Within the context of this paper, the constructed objective function F encapsulates the financial burden of running thermal generation units and distributed battery storage, in addition to the charges from carbon emissions attributable to both the thermal units and the PEVs. The analysis, however, omits the cross-temporal interdependencies that may exist among hourly cost components. The formulation reads as follows:

$$\begin{cases} F = \omega Cost + (1-\omega)\, Emission \\ Cost = min\ (f_{UC} + f_{bat}) \\ Emission = min(f_{UC}^{emi} + f_{PEV}^{emi}) \end{cases} \quad (1)$$

In **Eq. 1**, the expenditure tied to the units' power output separates into two portions: the fuel consumed during operational periods, and the expenses incurred when bringing units online or offline. The emission-related charges combine the $CO_2$ contributions from the thermal units $f_{UC}^{emi}$ and from the PEV fleet $f_{PEV}^{emi}$.

$$\begin{cases} f_{UC} = \sum_{t=1}^{T} \sum_{j=1}^{n} (F_j(P_{j,t}) z_{j,t} + ST_{j,t}(1 - z_{j,t-1}) z_{j,t}) \\ f_{bat} = \sum_{t=1}^{T} \sum_{k=1}^{nb} C_{k,t} \times pr \\ f_{UC}^{emi} = \sum_{t=1}^{T} \sum_{j=1}^{n} F_j^{emi}(P_{j,t}) z_{j,t} \times pr_e \\ f_{PEV}^{emi} = \sum_{t=1}^{T} \sum_{p=1}^{np} E_p^{PEV} \times pr_e \end{cases} \quad (2)$$

Where Pj,t captures the electric power dispatched by the jth unit in hour t. The cost of the fuel burned while the units are running is denoted by $Fj$ ($Pj$,). $F_j^{emi}$ represents the functional relationship translating unit emissions into a monetary cost. $Ck$, specifies the storage capacity of the kth battery at each hourly step.  denotes the aggregate capacity pooled across the PEV fleet. pr and pre stand for the unit price of battery installation and the prevailing average emission trading valuation, respectively, as put forward by Ref. [58]. $\omega$ serves as the weighting factor that steers the compromise between economic savings and emission curtailment, assigned a value of 0.3 in this study.

The fuel expenditure curve and the emission costing curve are displayed in **Eqs. 3 and 4:**

$$F_{j,t}(P_{j,t}) = a_j + b_j P_{j,t} + c_j P_{j,t}^2 \quad (3)$$

© 2023 The Author(s). | Published by Institute of Smart Energy Systems Press

$$F_{j,t}^{emi}(P_{j,t}) = \alpha_j + \beta_j P_{j,t} + \gamma_j P_{j,t}^2 \quad (4)$$

Where aj, bj, and cj denote the fuel-related coefficients belonging to the jth unit. αj, βj, and $\gamma$j designate the $CO_2$ emission coefficients for the jth unit.

Reflecting the physical traits of the generating hardware, most units may need to observe restrictions on state transitions, such as a mandatory waiting period before a restart following shutdown. The startup–shutdown cycle drains extra fuel during ignition, so the startup expenditure must be reflected in the economic objective, expressed as $ST_j(1 - z_{j,t-1})z_{j,t}$, and structured through the model below:

$$ST_{j,t} = \begin{cases} ST_j^{hot}, \ if \ MDT_j \le CDT_{j,t} \le MDT_j + T_{cold,j} \\ ST_j^{cold}, \ if \ CDT_{j,t} > MDT_j + T_{cold,j} \end{cases} \quad (5)$$

Where $zj$, is a binary indicator capturing whether the jth unit stands in the on state (1) or the off state (0) at time t. If the unit was offline during the prior interval but switches online for the current one, the startup charge is levied; otherwise, the charge is set to zero. The startup charge can be further differentiated into a hot start rate or a cold start rate, governed by the length of the idle period the unit has experienced before reactivation. $CDTj$, and $MDTj$ reflect the uninterrupted idle duration and the mandated minimum idle duration for the jth unit, respectively. The threshold delineating cold start eligibility is given by $T_{cold,j}$. $ST_j^{hot}$ and $ST_j^{cold}$ correspond to the hot-start regime and the cold-start regime, respectively. When the unit's offline duration surpasses $MDTj$ yet stays beneath the sum of $MDT_j + T_{cold,j}$, the startup is classed as a hot start; otherwise, the cold start classification applies.

## Constraints of the proposed problem

Determining the number of units to commit across successive time blocks requires consideration of numerous parameters to achieve peak performance. These considerations encompass the boundary conditions of individual units and the temporal linkages that couple decisions across hours. Conformity with these constraints is fundamental to securing the lowest feasible economic cost. In addition, the footprint of DGs and PEVs is likewise embedded within the constraint set.

### Power balance constraints

The demand for electrical power in industrial settings varies continuously. Added to this, the injection of DGs and PEVs into the grid modifies its energetic makeup, necessitating explicit consideration of equilibrium conditions, as captured in the following expression:

$$\sum_{j=1}^{n} P_{j,t} z_{j,t} + \underbrace{P_{PV,t} + P_{Bat,t}}_{DGs} = P_{D,t} + P_{PEV,t} \quad (6)$$

In **Eq. 6**, the combined output from the full set of committed units during hour t is captured by $\sum_{j=1}^{n} P_{j,,}$, $P_{D,t}$ corresponds to the baseline consumer load at time t; the distributed storage component breaks down into $P_{PV,t}$ and $P_{Bat,t}$, which signify the grid-tied photovoltaic infusion and the discharge from batteries on the supply side at hour t, respectively. $P_{PEV,t}$ describes the charging demand originating from the PEV pool during hour t, which can operate in a dual-mode fashion: grid-to-vehicle (G2V) and vehicle-to-grid (V2G) [59]. The PEVs either absorb electric power from the network to replenish their batteries or can feed power backward into the grid as circumstances warrant. Stated more directly, the consumption power of PEVs is registered as a positive quantity, whereas the power they inject for grid-support services is logged as a negative quantity.

© 2023 The Author(s). | Published by Institute of Smart Energy Systems Press

## Constraints of generating capacity

The physical characteristics of generation assets impose hard ceilings and floors on their productive output, which must be reflected in the model. Additionally, since the formulation jointly considers DGs alongside UC, the operational headroom of both the solar arrays and the battery installations must be bounded, yielding the restrictions articulated below:

$$z_{j,t} P_{j,min} \leq P_{j,t} \leq z_{j,t} P_{j,max} \quad (7)$$

$$0 \leq P_{PV,t} \leq P_{PV,max} \quad (8)$$

$$P_{Bat,min} \leq P_{Bat,t} \leq P_{Bat,max} \quad (9)$$

In **Eq. 7**, $Pj$, and $Pj$, mark the lowest and highest power injection limits tied to the jth unit, respectively. The productive potential of photovoltaic panels is dictated predominantly by ambient variables—solar radiation chief among them—and by the scale of the deployed array; for this investigation, the installed PV capacity is permitted to vary within the band [0, $P_{PV,max}$ ], as shown in **Eq. 8**. $P_{Bat,min}$ and $P_{Bat,max}$ designate the battery's minimum permissible capacity [MW] and its maximum permissible capacity [MW], respectively.

## Spinning reserve constraints

In everyday power system operation, earmarking a contingent of readily dispatchable capacity is essential to accommodate unforeseen load swings and deviations between forecasted and actual demand. This operational prerequisite is rendered mathematically as follows:

$$\sum_{j=1}^{n} P_{j,max} z_{j,t} + P_{PV,t} + P_{Bat,t} \geq P_{D,t} + P_{PEV,t} + SR_t \quad (10)$$

$$SR_t = m \times P_{D,t}. \quad (11)$$

Where SRt captures the quantum of spinning reserve set aside for each hourly interval, with its calculation detailed in **Eq. 11**. The joint output delivered by the generating units and the DGs must not fall short of the sum of total consumer load and the spinning reserve buffer, thereby preserving supply integrity. This study embraces the advisory put forth by Ref. [60], configuring the spinning reserve at a magnitude of 0.1 times the conventional load profile.

## Minimum up or down time of units

The processes of unit decommitment and subsequent recommitment absorb both time and financial resources. If the gap separating shutdown from restart is compressed excessively, the machinery will undergo repetitive cycling, driving up fuel burn and associated charges. By embedding these temporal stipulations directly into the scheduling logic, the active intervals of the units can be rationally sequenced, trimming energy waste and cost, as formalized by:

$$z_{j,t} = \begin{cases} 1, & if\ 1 \leq CUT_{j,t-1} < MUT_j \\ 0, & if\ 1 \leq CDT_{j,t-1} < MDT_j \\ 0\ or\ 1, & otherwise \end{cases} \quad (12)$$

© 2023 The Author(s). | Published by Institute of Smart Energy Systems Press

In **Eq. 12**, the binary on–off status is coded using the integers 0 and 1, wherein MUTj and MDTj reflect the shortest duration a unit must remain continuously energized and continuously de-energized, respectively. $CUTj$,-1 logs the accumulated uptime and CDT$j$,-1 logs the accumulated downtime of the units. Should a unit find itself in the running state for a period shorter than the mandated minimum uptime, it is forced to stay online; the converse requirement holds on the shutdown side.

### Constraints of PEVs

Because the charging appetite of the PEV collective is stochastic by nature, imposing bounds on their operation becomes a prerequisite for preserving grid stability. These bounds include extreme limits on charging and discharging throughput, as well as fleet-level energy requirements, both expressible via **Eqs. 13 and 14**, respectively.

$$P_{PEV\,D,t,max} \le P_{PEV\,J} \le P_{PEVC,t,max} \quad (13)$$

Where $P_{PEV\ D,,x}$ and $P_{PEV\ C,t,max}$ denote the absolute maximum discharge throughput and the absolute maximum charge throughput achievable by the aggregated PEV ensemble within any single hour, respectively.

$$\sum_{t=1}^{T} P_{PEV\,J} = P_{PEV,total} \quad (14)$$

**Eq. 14** codifies the total quantum of electrical energy indispensable for the PEV fleet to execute its regular daily functioning. At the same time, , encapsulates the entirety of the charging load demanded by all PEVs over the course of that day.

### State of charge limit of battery

The electrochemical makeup of the storage batteries necessitates vigilant oversight of their SoC, given that both deep discharge and sustained overcharge degrade their usable life. Accordingly, a bounded operating envelope must be established for the battery SoC, which can be delineated as:

$$SoC_{min} \le SoC_{k,t} \le SoC_{max} \quad (15)$$

Where $SoCmin$ stands for the absolute floor on the SoC applied uniformly across the energy storage fleet, pegged at 10%, and $SoCm$ax stands for the absolute ceiling, pegged at 100%.

# Materials and Methods

The system configuration advanced in this work—coupling thermal units with DGs and PEVs—manifests high dimensionality, pronounced multimodality, deep-seated coupling, and marked nonlinearity, traits that collectively stymie classical optimization solvers. To overcome these hurdles, this paper introduces a binary level-based learning swarm optimization framework.

## Original level-based learning swarm optimization

The computational intensity inherent in cracking the MESSs scheduling formulation escalates as the variable count climbs. Concurrently, the solution landscape, encompassing every conceivable candidate, mushrooms exponentially, rendering exhaustive traversal increasingly unattainable. When confronting tightly interlinked, high-dimensional formulations, the optimizers SLPSO [61] and CSO [62] exploit the topmost individuals residing in the current population to

© 2023 The Author(s). | Published by Institute of Smart Energy Systems Press

steer the evolutionary trajectory of the remainder, a ploy that augments heterogeneity and bolsters their high-dimensional efficacy. Nevertheless, both these algorithms confine themselves to a single topmost individual as the guiding beacon, and the collective pool of individuals shares an averaged population-wide coordinate. This structural choice constrains the attainable diversity uplift during each successive update sweep.

The level-based learning paradigm is the cornerstone of level-based learning swarm optimization (LLSO), which involves stratifying the particle assembly into distinct echelons. Moreover, it taps the intelligence of the two fittest exemplars within the population to guide the learning of the subordinate members, thereby amplifying their capacity to home in on the globally optimal solution. In addition, the scheduling optimization for MESSs constitutes a nonlinear mixed-integer program. The binary choice variables map onto the activation and deactivation statuses of the generating units. In contrast, the handling of PEV load profiles and DRG infeed operates on continuous decimal-valued domains. Consequently, a refined LLSO variant is sculpted in this paper to tune the binary on–off flags of the units in alignment with the needs of real-world application.

## Improved LLSO

Initially, the members forming the population are rank-ordered according to an ascending sort of their fitness metrics, in a manner akin to SLPSO. They are then uniformly assigned to distinct echelons (L1, L2, L3, and L4), after which each member selects two other members at random from two separate higher echelons to serve as exemplars for its positional refresh.

Once the fitness scores are evaluated and sorted, let the population N be apportioned across M levels, with each level annotated as $Lm$ = [$L1$, $L2$, …, $LM$]. A loftier level houses fitter members and bears a smaller numerical index. By way of illustration, members populating L3 dominate those in L4 in terms of quality. The headcount within any single level is fixed at S, where S = N/M. Crucially, as a protective measure against corrupting the most prospective members, those assigned to L1 are held static, bypassing the update phase and proceeding intact into the subsequent generation. The learning protocol through which population positions are refreshed under LLSO is dictated by:

$$\mathbf{X}^d(t+1) = \begin{bmatrix} x^d_{1,1} + v^d_{1,1}(t+1) & x^d_{1,2} + v^d_{1,2}(t+1) & \cdots & x^d_{1,S} + v^d_{1,S}(t+1) \\ x^d_{2,1} + v^d_{2,1}(t+1) & x^d_{2,2} + v^d_{2,2}(t+1) & \cdots & x^d_{2,S} + v^d_{2,S}(t+1) \\ \vdots & & \ddots & \\ x^d_{M,1} + v^d_{M,1}(t+1) & x^d_{M,2} + v^d_{M,2}(t+1) & \cdots & x^d_{M,S} + v^d_{M,S}(t+1) \end{bmatrix} \quad (16)$$

In **Eq. 16**, $\mathbf{X}d$ ($t$ + 1) represents the population projected along the dth dimension. Every member recalibrates its position following **Eqs. 17 and 18.**

$$x^d_{i,j}(t+1) = x^d_{i,j} + v^d_{i,j}(t+1) \quad (17)$$

Where $x^d_{i,j}(t)$ designates the location of the jth member along the dth dimension that belongs to the ith level Li, and $v^d_{i,j}$ designates its corresponding velocity at generation t.

$$v^d_{i,j}(t+1) = r_1(t)v^d_{i,j}(t) + r_2(t)\Delta x^d_{l_1,j}(t) + \phi r_3(t)\Delta x^d_{l_2,j}(t) \quad (18)$$

With:

© 2023 The Author(s). | Published by Institute of Smart Energy Systems Press

$$\begin{cases} \Delta x_{l_1,j}^d(t) = x_{l_1,k_1}^d(t) - x_{i,j}^d(t) \\ \Delta x_{l_2,j}^d(t) = x_{l_2,k_2}^d(t) - x_{i,j}^d(t) \\ \phi = 0.01 \times \frac{n}{m} \end{cases} \quad (19)$$

In **Eq. 18,** $\Delta x_{l_1,j}^d$ (*t*) and $\Delta x_{l_2,j}^d$ (*t*) constitute the informational gains absorbed by the member from two separate superior exemplars during each generational cycle. $x_{l_1,j}^d$ (*t*) and $x_{l_2,j}^d$(*t*) correspond to the two exemplars extracted from two separate chosen levels, LI1 and LI2; l1 and l2 are the level identifiers drawn from two separate higher echelons residing within the bracket [1, i-1]. The placeholders k1 and k2 are randomly drawn from the span [1, LS] to pinpoint two distinct members. r1(t), r2(t), and r3(t) are uniformly sampled from the unit interval [0,1]. ϕ functions as the weighting coefficient that tempers $\Delta x_{l_2,j}^d$(*t*); its magnitude is shaped by contextual factors like population size and problem dimensionality, and it regulates the intensity with which the present member revises itself when gleaning information from a comparatively weaker source. Of note, the index of L2 stands higher than that of L1, but both are lower—hence better—than the index of Li.

Given that the unit status undergoing optimization during the update procedure is binary in character. At the same time, the freshly computed particle velocity values remain decimal; it is imperative to impose a uniform encoding discipline across all particle attributes within the update framework. To achieve this, a V-shaped transfer mapping is employed in this study to discretize the particles at each refreshed coordinate. The adapted LLSO update scheme emerges as follows:

$$x_{i,j}^d(t+1) = x_{i,j}^d + BC(v_{i,j}^d(t+1)) \quad (20)$$

$$BC(v_{i,j}) = 2 * \left| \frac{1}{1+e^{-v_{i,j}}} - 0.5 \right| \quad (21)$$

Examining (21), it becomes clear that the particle velocity $v$ is the decisive factor steering the discretization outcome. When the velocity magnitude drifts too high or too low, the individual's position tends to saturate at 0 or 1. To prevent this, the velocity is confined within the corridor [−4,4] in the present work. The companion positional update for the individual then unfolds as:

$$x_{i,j} = \begin{cases} 1, & \text{if } rand < BC(v_{i,j}) \\ 0, & \text{otherwise} \end{cases} \quad (22)$$

Where xi,j signals the discretized, post-conversion position of the individual; rand produces a uniformly distributed random variate spanning [0,1]. Whenever ($vi$,) surpasses the randomly drawn integer rand, the particle's positional attribute is set to 1, indicating that the unit is brought online in the context of the UC problem. Otherwise, the attribute is set to 0, signaling that the unit remains offline.

© 2023 The Author(s). | Published by Institute of Smart Energy Systems Press

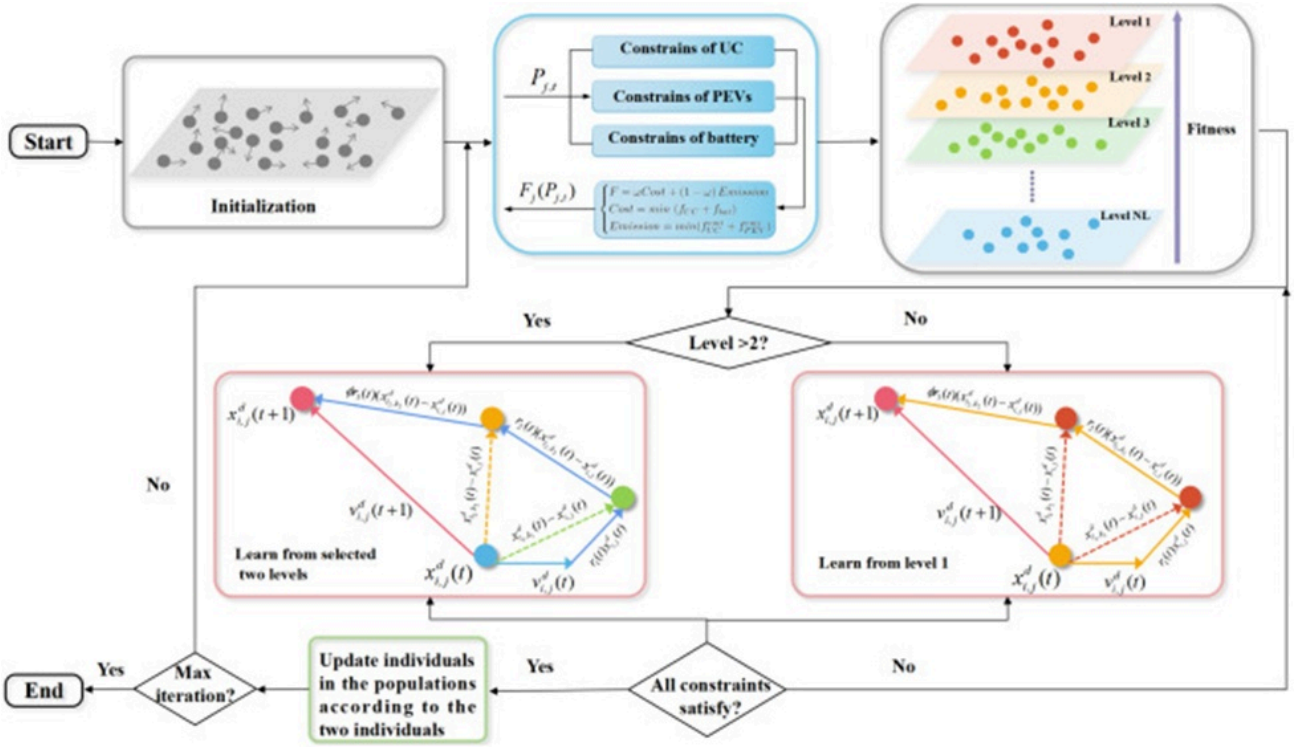


**Figure 2.** The algorithm flowchart of BLLSO.

The tiered learning architecture may steer members stationed in the upper echelons toward intensified local refinement, while members in the lower echelons veer toward broader canvassing of the search domain. From one vantage point, this can foster a healthy trade-off between exploitative and exploratory behaviors tailored to each member. From another angle, the stochastic elements embedded in level picking and dominant exemplar selection contribute positively to diversity preservation—a factor of paramount significance in large-scale optimization undertakings. The algorithm flowchart of BLLSO is shown in **Figure 2.**

## The specific stages of the proposed algorithm

As PEV adoption continues its upward trajectory, the charging demands of an expansive PEV fleet threaten to strain the electricity network, thereby underscoring the need for effective control strategies to uphold energy equilibrium and to fortify the grid's dependability and performance. In parallel, photovoltaic panels and battery banks are integrated into the grid as distributed energy storage. This move introduces volatility into the supply side owing to the capriciousness of disparate energy sources. Anchored by these concerns, a binary level-based learning swarm optimization methodology is formulated, and the comprehensive MESSs scheduling framework is condensed in **Figure 3.** The step-by-step execution of the proposed MESSs optimization algorithm for UC problems meshed with DGs and PEVs proceeds as follows:

(1) Data initialization: The first step involves feeding in and initializing the datasets describing the thermal units along with the round-the-clock charging traces of the PEVs. A collection of indispensable parameters likewise demands initialization, among them the ceiling and floor of generation output, the hot and cold start expenditure rates, the fuel cost constants, and the starting commitment status of every unit. The permissible velocity envelope for the particles and the algorithm control parameters that will govern the optimization loop are also among the entities subject to initialization.

© 2023 The Author(s). | Published by Institute of Smart Energy Systems Press

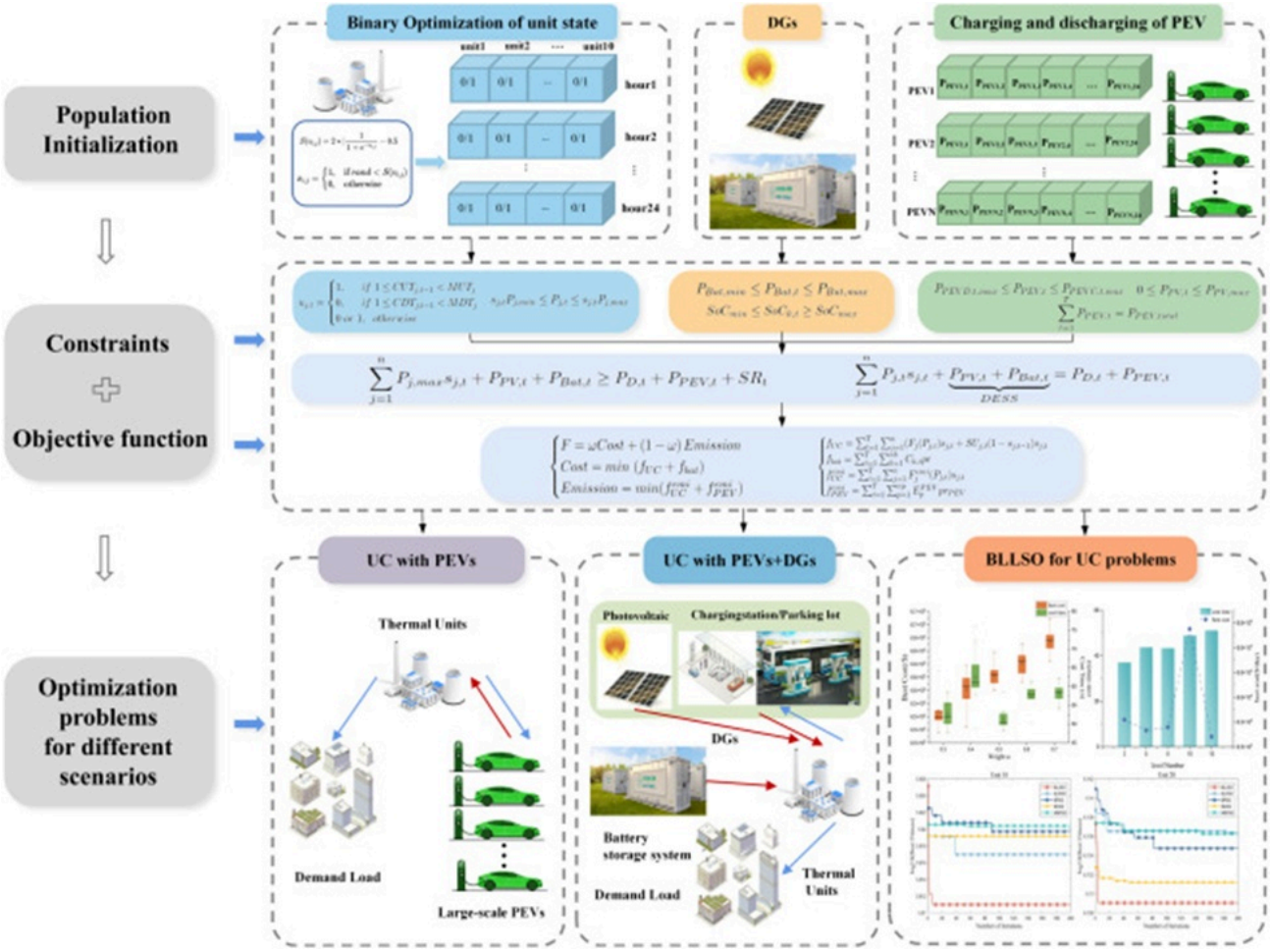


**Figure 3.** The proposed MESSs scheduling framework.

(2) Constraint handling: To safeguard the fidelity and robustness of the optimization exercise, constraint enforcement constitutes an obligatory stage. The initialized unit data are compelled to respect the minimum up/down-time thresholds; where violations are detected, the on–off status of the offending unit is clamped to the applicable boundary. The PEV data must conform to the requirements laid out in (13) and (14). The battery must stay within the prescribed SoC window to forestall both excessive depletion and overcharging.

(3) Fitness calculation: In accordance with expression (1), the fitness score attached to each particle is evaluated, and the lambda iteration technique [19] is invoked to determine the dispatch of each unit. It bears mentioning that distinct scenarios may call for different instantiations of the objective function.

(4) Individual stratification: Upon deriving the fitness scores for the entire particle set, the particles are ranked in ascending order and subsequently apportioned into strata based on their fitness standings. To reiterate, the particles occupying the topmost level L1 are carried forward into the next iteration untouched by any update or learning process—a safeguard intended to prevent the corruption of the most auspicious candidates. Particles positioned in level L2 renew their coordinates by modeling themselves after two superior individuals, both of which are sourced exclusively from level L1.

(5) Population update: The BLLSO optimization engine is set into motion to refine the coordinates of all individuals, steered by their fitness valuations. Particles that have undergone positional modification must subsequently be rechecked for conformity with all constraints.

© 2023 The Author(s). | Published by Institute of Smart Energy Systems Press

(6) Judging the termination condition: If the running tally of completed iterations falls short of the prescribed termination iteration ceiling, the algorithm cycles back to stages (3) through (5). If the ceiling has been met, the optimal result found is emitted, and the execution is brought to a close.

# Numerical Studies and Results Analysis

This section presents a collection of case studies to verify the soundness and feasibility of the recommended optimization architecture. The first case tests whether regulated PEV charging and discharging can effectively trim consumption peaks and fill demand troughs on the electricity network. The second case pivots to evaluating how the proposed MESSs components behave individually and collectively, aiming to clarify what part each module plays and what value it delivers to grid operations. The final case is designed to exhibit the commanding edge held by the LLSO algorithm when applied to UC formulations spanning multiple unit fleet dimensions, with its performance measured against four competing algorithms.

## Experimental setup

The PEV-related data originates from the daily charging demand trace of 50,000 electric vehicles operating in Shenzhen, Guangdong Province, China, captured over a standard 24-hour cycle. The complete set of experiments was run on a desktop machine fitted with a 12th Gen Intel(R) Core(TM) i7-12700 CPU clocked at 2.10 GHz, equipped with 32 GB of RAM, and operating under the MATLAB R2022b software environment. The defining constants for the thermal generation units adopted in this investigation follow the specifications documented in Ref. [63], whose exhaustive details are collated in **Table 1**. A point worth stressing is that expanding the unit count proportionally increases the problem's dimensionality. For a fleet of 10 units, the decision variable vector spans 240 dimensions; inflating the fleet to 100 units balloons the dimensionality to 2400.

**Table 1.** UC model parameter settings.

| Empty cell | **Unit10** | **Unit9** | **Unit8** | **Unit7** | **Unit6** | **Unit5** | **Unit4** | **Unit3** | **Unit2** | **Uni** |
|---|---|---|---|---|---|---|---|---|---|---|
| **Pmax(MW)** | 55 | 55 | 55 | 85 | 80 | 162 | 130 | 130 | 455 | 45 |
| **Pmin(MW)** | 10 | 10 | 10 | 25 | 20 | 25 | 20 | 20 | 150 | 15 |
| **a($ /h)** | 670 | 665 | 660 | 480 | 370 | 450 | 680 | 700 | 970 | 100 |
| **b($ /MWh)** | 27.79 | 27.27 | 25.92 | 27.74 | 22.26 | 19.7 | 16.5 | 16.6 | 17.26 | 16.1 |
| **c($ /MW$^2$h)** | 0.00173 | 0.00222 | 0.00413 | 0.00079 | 0.00712 | 0.00398 | 0.00211 | 0.002 | 0.00031 | 0.000 |
| $\alpha$**(ton/h)** | 360.0012 | 350.0056 | 330.0056 | 330.0056 | 320.0006 | 320.0006 | 300.3910 | 300.3910 | 103.3908 | 103.3 |
| $\beta$**(ton/MW h)** | −3.9864 | −3.9524 | −3.9023 | −3.9023 | −3.8132 | −3.8132 | −4.0695 | −4.0695 | −2.4444 | −2.4 |
| $\gamma$**(ton/MW$^2$h)** | 0.047 | 0.0465 | 0.0465 | 0.0465 | 0.0344 | 0.0344 | 0.0509 | 0.0509 | 0.0312 | 0.03 |
| **MUT(h)** | 1 | 1 | 1 | 3 | 3 | 6 | 5 | 5 | 8 | 8 |
| **MDT(h)** | 1 | 1 | 1 | 3 | 3 | 6 | 5 | 5 | 8 | 8 |
| ***SU$_H$* ($)** | 30 | 30 | 30 | 260 | 170 | 900 | 560 | 550 | 5000 | 450 |
| ***SU$_C$* ($)** | 60 | 60 | 60 | 520 | 340 | 1800 | 1120 | 1100 | 10 000 | 900 |
| ***T$_{cold}$* (*h*)** | 0 | 0 | 0 | 2 | 2 | 4 | 4 | 4 | 5 | 5 |

© 2023 The Author(s). | Published by Institute of Smart Energy Systems Press

| | | | | | | | | | | |
|---|---|---|---|---|---|---|---|---|---|---|
| **Initial Status(h)** | 0 | 0 | 0 | 0 | 0 | 0 | 0 | 0 | 1 | 1 |

## The influence of management of PEVs charge and discharge on UC problems

This segment dissects the consequences of folding electric vehicle charge/discharge regulation into the electrical power system. On one flank, PEVs represent a dispatchable load resource that can be programmed to absorb energy during nighttime or other low-demand slots when overall consumption wanes, a flexibility that aids load balancing and helps the grid weather peak consumption periods. On the opposite flank, stationary batteries hold a vital position inside distributed storage architectures, since they enable the retention of excess generation when supply outstrips demand and its subsequent release when consumption climbs. This functionality contributes meaningfully to grid steadiness.

The experimental configuration posited in this paper pairs a 10-unit generation fleet with a pool of 150,000 PEVs, stipulating that each PEV carries a 30 KWh battery [64], the upper power bound of the stationary storage batteries is fixed at 5 MW [65], and the collective PEV energy requirement approximates 1.114 GWh. Beyond this, the extreme charging and discharging power envelopes for the aggregated PEVs are set to 153 MW and −153 MW, respectively; the portion of PEV battery capacity deemed usable is 50%, while the hourly availability ratio of the PEV stock is 20%.

The refined dispatch produced by the PEV charge/discharge management scheme embedded in the power grid is cataloged in **Table 2**. Per **Table 2**, the consumption crests materialize during the window spanning 9:00 am to 14:00 and again from 20:00 to 21:00, and the generating units' production peaks correspondingly cluster within those identical time bands. Additionally, when the system load sits at its apex, PEVs inject power to help satisfy the electrical appetite. When the load recedes to its nadir, PEVs switch to absorbing power. This behavior validates that the designed optimization routine successfully governs the PEV charge/discharge cadence and that PEVs can execute peak-shaving and valley-filling to flatten the demand profile. **Figure 4** lays side by side the unit output distributions under conditions with and without PEV involvement. A glance at **Figure 4a** confirms that when PEVs are absent, Units 1 and 2 bear a disproportionate share of the generation burden and suffer from an unevenly spread load across the 24 hours compared with the remaining units. In sharp contrast, **Figure 4b** shows that grafting PEVs onto the grid markedly eases the generation strain on the units and imparts a more uniform and stable character to the broader power system.

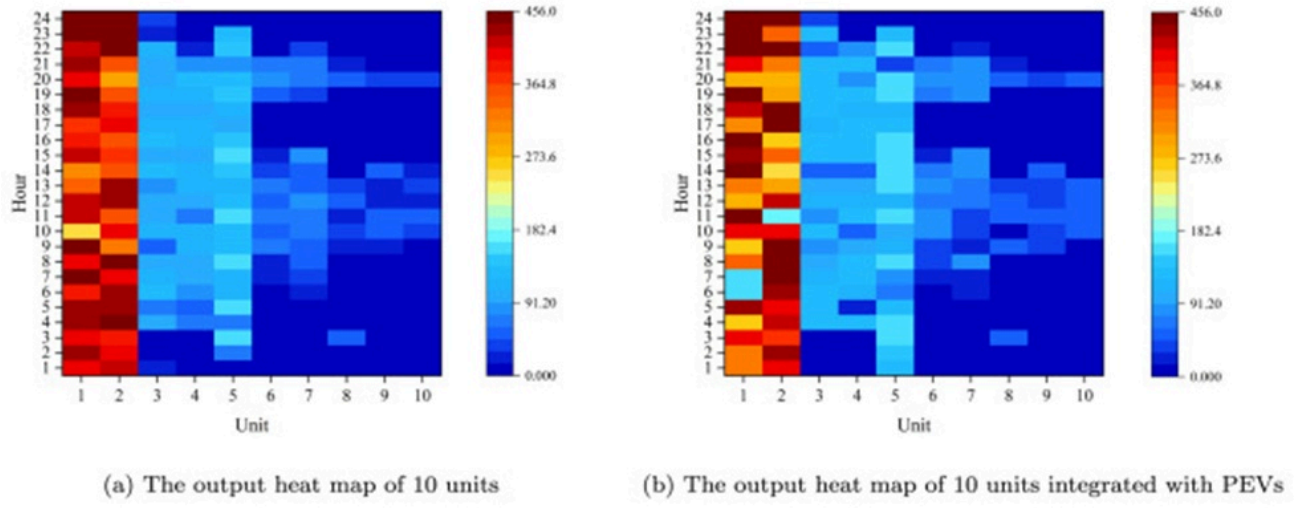


**Figure 4.** Heat map comparison of unit output under different scenarios.

© 2023 The Author(s). | Published by Institute of Smart Energy Systems Press

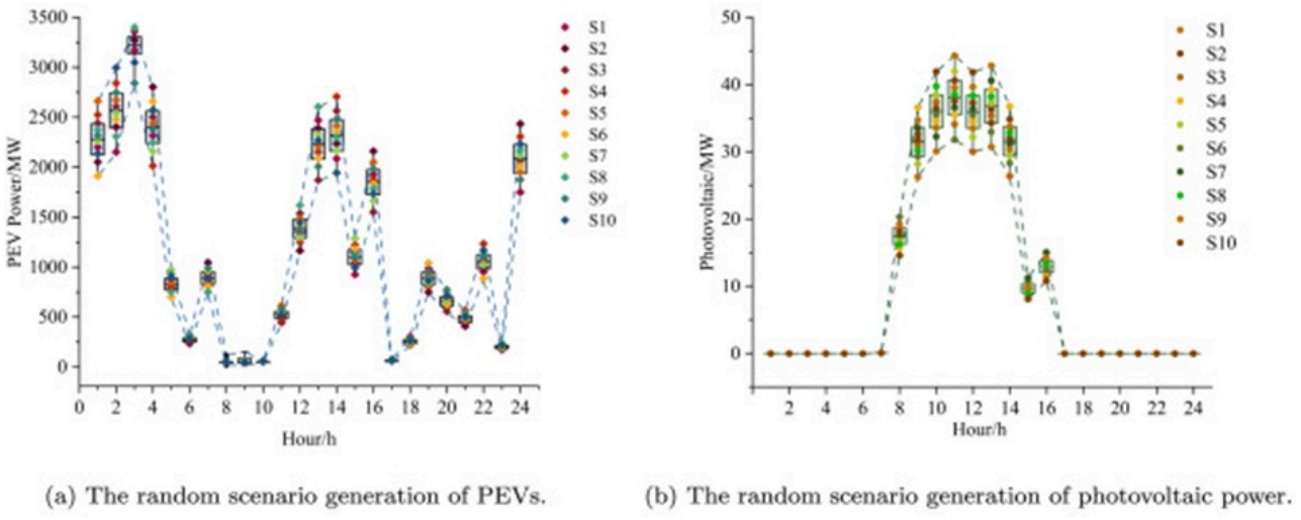


**Figure 5.** Scenario generation comparison of MESSs under 10 units.

**Table 2.** The optimal results of charge and discharge management of PEVs in UC problems.

| Hour | PEV Load (MW) | Demand (MW) | Unit10 (MW) | Unit9 (MW) | Unit8 (MW) | Unit7 (MW) | Unit6 (MW) | Unit5 (MW) | Unit4 (MW) | Unit3 (MW) | Unit2 (MW) | Unit1 (MW) |
|---|---|---|---|---|---|---|---|---|---|---|---|---|
| **1** | 153.00 | 700.00 | 0.00 | 0.00 | 0.00 | 0.00 | 0.00 | 0.00 | 20.00 | 0.00 | 450.22 | 382.78 |
| **2** | 153.00 | 750.00 | 0.00 | 0.00 | 0.00 | 0.00 | 0.00 | 0.00 | 49.80 | 0.00 | 455.00 | 398.20 |
| **3** | 153.00 | 850.00 | 0.00 | 0.00 | 0.00 | 0.00 | 0.00 | 0.00 | 20.00 | 73.57 | 454.43 | 455.00 |
| **4** | 153.00 | 950.00 | 0.00 | 0.00 | 0.00 | 0.00 | 0.00 | 101.07 | 45.19 | 85.00 | 453.57 | 418.16 |
| **5** | 138.35 | 1000.00 | 0.00 | 0.00 | 0.00 | 0.00 | 0.00 | 162.00 | 99.36 | 20.00 | 444.87 | 412.12 |
| **6** | 69.44 | 1100.00 | 0.00 | 0.00 | 10.00 | 0.00 | 0.00 | 88.47 | 129.40 | 117.58 | 384.14 | 439.85 |
| **7** | 121.29 | 1150.00 | 0.00 | 0.00 | 10.00 | 40.71 | 0.00 | 162.00 | 127.71 | 130.00 | 408.37 | 392.50 |
| **8** | 65.44 | 1200.00 | 0.00 | 0.00 | 0.00 | 61.57 | 48.02 | 126.88 | 130.00 | 107.39 | 409.84 | 381.74 |
| **9** | −59.38 | 1300.00 | 10.93 | 0.00 | 36.08 | 37.22 | 75.95 | 108.92 | 92.73 | 105.27 | 401.10 | 372.42 |
| **10** | −70.30 | 1400.00 | 18.29 | 52.57 | 30.41 | 77.22 | 58.09 | 92.46 | 130.00 | 79.35 | 387.05 | 404.25 |
| **11** | −76.03 | 1450.00 | 35.34 | 37.60 | 25.71 | 68.57 | 39.63 | 150.86 | 92.02 | 130.00 | 378.98 | 415.26 |
| **12** | −153.00 | 1500.00 | 10.00 | 46.92 | 10.00 | 85.00 | 66.40 | 122.98 | 130.00 | 105.49 | 434.00 | 336.21 |
| **13** | −94.19 | 1400.00 | 45.89 | 35.38 | 16.69 | 57.92 | 54.22 | 103.81 | 89.31 | 72.46 | 379.66 | 450.48 |
| **14** | −49.79 | 1300.00 | 0.00 | 19.57 | 33.78 | 63.77 | 56.03 | 100.58 | 70.01 | 110.20 | 389.92 | 406.35 |
| **15** | 77.53 | 1200.00 | 0.00 | 0.00 | 0.00 | 69.74 | 20.00 | 138.06 | 111.27 | 78.88 | 435.71 | 423.86 |
| **16** | 91.61 | 1050.00 | 0.00 | 0.00 | 0.00 | 25.00 | 0.00 | 82.29 | 84.02 | 130.00 | 385.01 | 435.27 |
| **17** | 72.26 | 1000.00 | 0.00 | 0.00 | 0.00 | 25.00 | 0.00 | 123.93 | 105.00 | 43.34 | 378.94 | 396.05 |
| **18** | 72.28 | 1100.00 | 0.00 | 0.00 | 0.00 | 25.00 | 0.00 | 162.00 | 105.60 | 96.41 | 328.27 | 455.00 |

© 2023 The Author(s). | Published by Institute of Smart Energy Systems Press

| | | | | | | | | | | | | |
|---|---|---|---|---|---|---|---|---|---|---|---|---|
| **19** | 65.02 | 1200.00 | 0.00 | 0.00 | 0.00 | 25.00 | 60.42 | 109.06 | 98.68 | 128.99 | 438.53 | 404.33 |
| **20** | −96.24 | 1400.00 | 46.70 | 41.06 | 20.30 | 67.76 | 45.24 | 93.83 | 84.37 | 120.74 | 399.42 | 384.33 |
| **21** | −57.30 | 1300.00 | 0.00 | 20.56 | 10.00 | 85.00 | 80.00 | 67.68 | 75.65 | 102.90 | 379.37 | 421.54 |
| **22** | 79.23 | 1100.00 | 0.00 | 0.00 | 55.00 | 0.00 | 0.00 | 110.32 | 115.92 | 45.00 | 455.00 | 398.00 |
| **23** | 153.00 | 900.00 | 0.00 | 0.00 | 0.00 | 0.00 | 0.00 | 63.00 | 80.00 | 0.00 | 455.00 | 455.00 |
| **24** | 153.00 | 800.00 | 0.00 | 0.00 | 0.00 | 0.00 | 0.00 | 60.25 | 0.00 | 0.00 | 437.75 | 455.00 |

## Uncertainty analysis of proposed MESSs

Since solar generation is both intermittent and meteorologically sensitive, and the plug-in behavior of electric vehicles is inherently nondeterministic, sustaining grid equilibrium can become a demanding undertaking. To systematically gauge the uncertainty contributed by renewable infeed and EV fleet behavior, this study employs the Latin hypercube sampling (LHS) methodology [66] to draw randomized specimens from a multi-dimensional parameter domain.

Within this subsection, the 10-unit MESSs serves as the testbed, and a set of 10 randomized scenarios is produced to mimic the stochastic nature of photovoltaic output and PEV charging/discharging patterns, with the intent of evaluating the impact of such randomness on the MESSs. Scrutiny of **Figure 5a** points to a notable swell in power uptake across all sampled scenarios during specific time corridors, especially in the hours preceding 7 am and following 8 pm. These consumption bumps map onto conventional usage patterns associated with the morning and evening mobility peaks, synchronized with the populace traveling to and from their workplaces. Setting themselves apart from the strongly randomized PEV traces, the PV production curves depicted in **Figure 5b** follow a distinctly periodic pattern aligned with the daily rhythm of sunrise and sunset, emphasizing that atmospheric and weather variables are the principal shapers of realized solar yield. Thus, the approach can be validated as capable of effectively capturing the stochastic properties of PEV power draw and the discontinuous character of solar generation. In parallel, the analytical findings equip grid operators with the ability to forecast power requirements more precisely and to institute the requisite corrective measures for accommodating widespread PEV and PV penetration.

**Tables 3 and 4** provide a comparative breakdown of the operational economic burden shouldered by the MESS under two contrasting paradigms: the PEV-centric scenario and the Photovoltaic-centric scenario. The scenarios tabulated mirror a spectrum of MESS operating states synthesized through the LHS procedure. The empirical record shows that the PEV scenario consistently incurs appreciably smaller economic penalties than the PV scenario. A probable explanation for this divergence lies in the unpredictable, fluctuating output profile of solar energy, which erodes system stability when set beside the PEV scenario. Across every scenario examined, the presence of BESS pushes economic outlays upward, an increase that can largely be attributed to the upfront capital investment that BESS deployment commands.

Nevertheless, the addition of BESS seems to compress the spread of economic outcomes, as manifested by a narrowing of the standard deviation metric. In concrete terms, the best-case standard deviation appearing in **Table 3** under BESS integration contracts by $ 312.52 /day when stacked against the configuration that omits BESS. Along analogous lines, the contraction reported in **Table 4** amounts to $514.02/day. This compressed dispersion underlines BESS's capacity to make the MESS economically more resilient, most notably when the system is subjected to extreme operational regimes.

**Table 3.** Economic cost comparison of MESS with PEVs and BESS.

| **Scenario** | **UC+PEV+BESS** | | | | **UC+PEV** | | | |
|---|---|---|---|---|---|---|---|---|
| | **Std** | **Mean** | **Worst** | **Best** | **Std** | **Mean** | **Worst** | **Best** |
| **S1** | 644.53 | 666 028.56 | 666 484.32 | 665 572.81 | 4394.68 | 650 496.15 | 653 603.65 | 647 388.64 |

© 2023 The Author(s). | Published by Institute of Smart Energy Systems Press

| | | | | | | | | |
|---|---|---|---|---|---|---|---|---|
| **S2** | 3205.40 | 666 454.13 | 668 720.69 | 664 187.57 | 1542.78 | 649 597.03 | 650 687.94 | 648 506.12 |
| **S3** | 1648.85 | 663 862.82 | 665 028.74 | 662 696.90 | 3166.63 | 649 978.24 | 652 217.38 | 647 739.10 |
| **S4** | 557.77 | 662 699.46 | **663 093.87** | 662 305.06 | **629.35** | 649 891.68 | 650 336.69 | 649 446.66 |
| **S5** | 2938.33 | 664 414.76 | 666 492.47 | 662 337.04 | 7051.87 | 646 998.75 | 651 985.17 | **642 012.33** |
| **S6** | 7214.75 | **661 620.11** | 666 721.72 | **656 518.51** | 1227.07 | 649 017.79 | 649 885.46 | 648 150.12 |
| **S7** | **316.83** | 665 312.11 | 665 536.15 | 665 088.08 | 1892.31 | 646 223.09 | 647 561.15 | 644 885.02 |
| **S8** | 3465.16 | 665 101.67 | 667 551.91 | 662 651.44 | 3264.05 | **644 798.89** | **647 106.92** | 642 490.86 |
| **S9** | 3346.59 | 664 398.42 | 666 764.82 | 662 032.01 | 1513.41 | 650 129.38 | 651 199.52 | 649 059.24 |
| **S10** | 1266.86 | 665 141.82 | 666 037.63 | 664 246.01 | 2826.65 | 647 735.24 | 649 733.98 | 645 736.49 |

**Table 4.** Economic cost comparison of MESS with photovoltaic and BESS.

| **Scenario** | **UC+PV+BESS** | | | | **UC+PV** | | | |
|---|---|---|---|---|---|---|---|---|
| | **Std** | **Mean** | **Worst** | **Best** | **Std** | **Mean** | **Worst** | **Best** |
| **S1** | 5632.32 | 590 644.28 | 594 626.94 | 586 661.62 | 9634.49 | **571 775.92** | 578 588.54 | **564 963.30** |
| **S2** | 5722.28 | **590 067.14** | 594 113.40 | **586 020.88** | 6653.03 | 579 895.59 | 584 599.99 | 575 191.18 |
| **S3** | 472.89 | 593 349.61 | 593 684.00 | 593 015.23 | 3216.19 | 576 308.44 | **578 582.63** | 574 034.24 |
| **S4** | 1152.46 | 594 531.83 | 595 346.75 | 593 716.91 | 6570.93 | 579 045.97 | 583 692.32 | 574 399.62 |
| **S5** | **420.68** | 592 756.11 | **593 053.58** | 592 458.64 | 2537.18 | 579 153.04 | 580 947.11 | 577 358.98 |
| **S6** | 1511.78 | 594 362.31 | 595 431.31 | 593 293.32 | 9608.17 | 584 272.97 | 591 066.97 | 577 478.96 |
| **S7** | 1476.77 | 592 739.77 | 593 784.01 | 591 695.53 | 1650.72 | 583 238.23 | 584 405.47 | 582 071.00 |
| **S8** | 3817.39 | 595 221.20 | 597 920.51 | 592 521.90 | 4739.92 | 583 161.78 | 586 513.41 | 579 810.14 |
| **S9** | 3512.19 | 597 705.89 | 600 189.39 | 595 222.40 | 4724.35 | 583 177.16 | 586 517.78 | 579 836.54 |
| **S10** | 3504.66 | 595 265.79 | 597 743.97 | 592 787.62 | **934.70** | 583 770.81 | 584 431.75 | 583 109.88 |

## Benefit analysis for proposed MESSs

This section provides a comprehensive assessment of the repercussions of connecting photovoltaics and BESS, functioning as DGs, to the grid load and integrating them with PEVs within the UC modeling construct. The investigation is split into three distinct cases to examine and contrast the footprint of PEVs and DRGs on the grid, as well as the net benefits that MESSs bestow upon the electrical infrastructure; the case delineations are spelled out in **Table 5**. The solar irradiance-to-power conversion data employed in this investigation correspond to a full 24-hour cycle in Shenzhen.

**Figure 6** displays the sensitivity of unit loading to varying battery SOC thresholds. It is readily observable that when the battery SOC sits at the elevated 90% mark, the burden on the units registers lower than when SOC stands at the depleted 0% level across the preponderance of the day's hours. The underlying reason is that the battery can execute

© 2023 The Author(s). | Published by Institute of Smart Energy Systems Press

intelligent energy arbitrage, discharging previously accumulated reserves when the system enters peak demand phases. By the same token, BESS can help curb the volume of $CO_2$ emitted per unit of fossil-derived electricity. Hence, jointly weaving PEVs and BESS into the system fabric proves constructive for disentangling the tightly enmeshed UC puzzle.

**Table 5.** Scenario settings.

| Case | Scenario description |
|---|---|
| Case 1 | Unit Commitment (UC) framework incorporating Plug-in Electric Vehicles (PEVs). |
| Case 2 | UC framework integrated with both PEVs and Photovoltaic (PV) generation. |
| Case 3 | UC framework combining PEVs, PV generation, and a Battery Energy Storage System (BESS). |

The definitive optimized results from jointly incorporating DGs and PEVs into the UC formulation are assembled in **Figure 7**. In contrast, **Table 6** tabulates the side-by-side comparison of the outcomes produced by the three distinct UC cases. Extracting from **Table 6** and zeroing in on the economic toll of unit operation, the combined outlay for fuel and carbon emissions tallied in case 3 lands at 638540.54 $/day, a figure that falls beneath case 2 by 2610.49 $/day and beneath case 1 by 12852.61 $/day. The conclusion follows naturally that the fusion of PEVs and DGs can trim both the expense of generating electricity and the $CO_2$ footprint attributable to the grid.

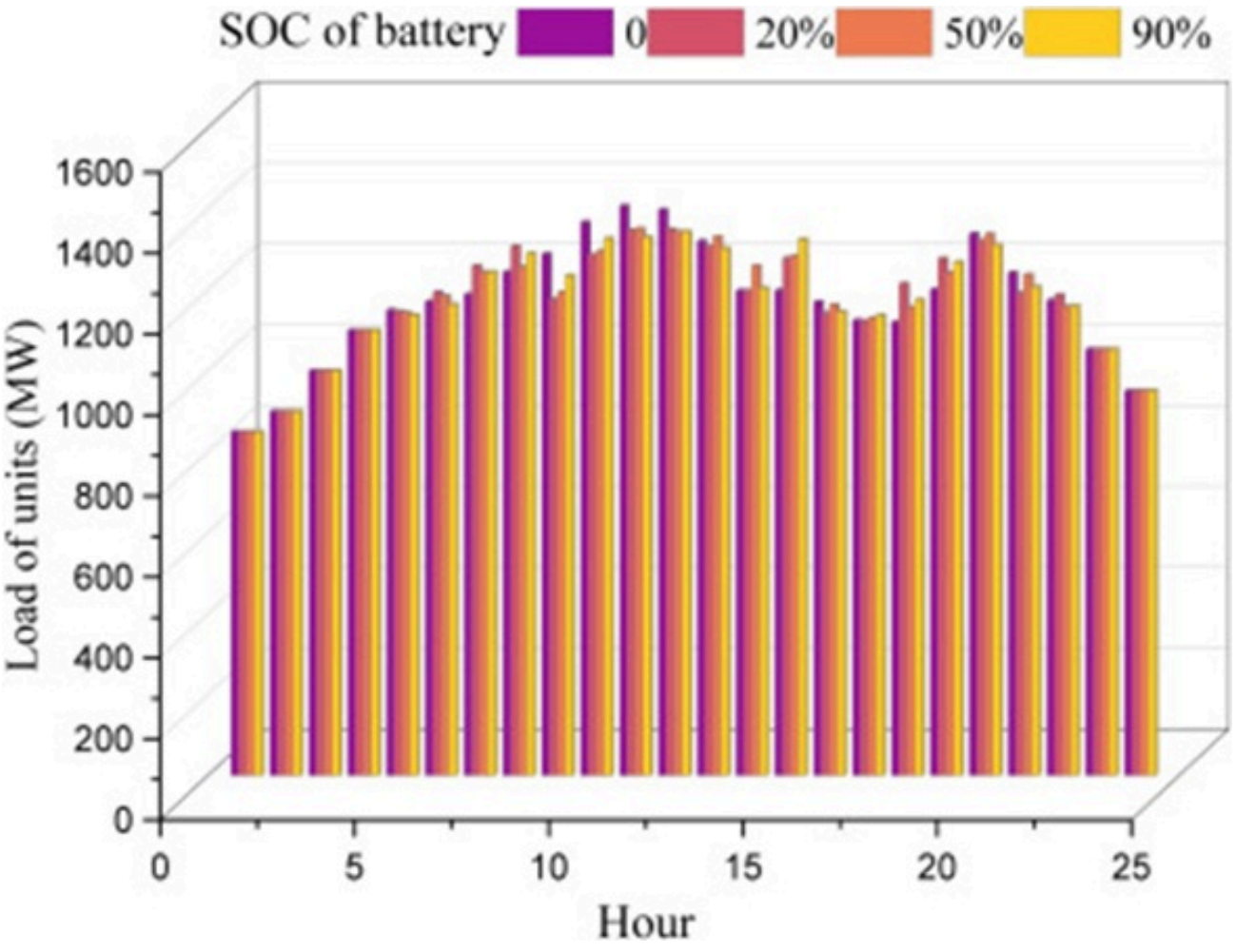


**Figure 6.** The influence of various SOC of battery for UC problems.

© 2023 The Author(s). | Published by Institute of Smart Energy Systems Press

**Figure 7b** plots the total hourly power contribution of the 10 units mapped over a complete 24-hour cycle. Zooming in on case 3, the plot makes it unmistakable that during the demand zenith at 12:00 am, the power drawn from the units experiences a considerable contraction compared to case 2 by 66.69 MW and compared to case 1 by 102.34 MW. This evidence certifies that embedding photovoltaics into the grid produces a constructive effect and yields savings in generation outlays. Furthermore, the aggregate curve for case 3 appears visibly less jagged than those of the other two cases, which strongly illustrates that integrating PEVs with DGs improves the electricity grid's dependability. Turning to **Table 7,** at 12:00 am—the hour of peak consumption—the discharge contribution of the PEV fleet registers 78.7 MW below the corresponding figure in **Table 2**, implying that the introduction of DGs also assists in the orchestration of PEV charging and discharging. Placing **Table 2** alongside **Table 7**, it becomes conspicuous that at 12:00, the dispatched output of the first 5 units listed in **Table 2** vaults past 100 MW and that of the trailing 5 units stands at a minimum of 10 MW. In contrast, in **Table 7**, merely two units breach the 100 MW mark. This result corroborates that DGs can take pressure off the generating units' demand burden and heighten the reliability of the electric grid, all without failing to satisfy the load.

**Table 6.** Cost comparison for different cases.

| Case | Difference | Carbon emission cost/($/day) | Difference | Economic cost/($/day) |
|---|---|---|---|---|
| **Case 1** | – | 656 881.77 | – | 651 393.15 |
| **Case 2** | 2.51% | 640 398.12 | 1.57% | 641 151.03 |
| **Case 3** | 2.72% | 638 998.57 | 1.97% | 638 540.54 |

© 2023 The Author(s). | Published by Institute of Smart Energy Systems Press

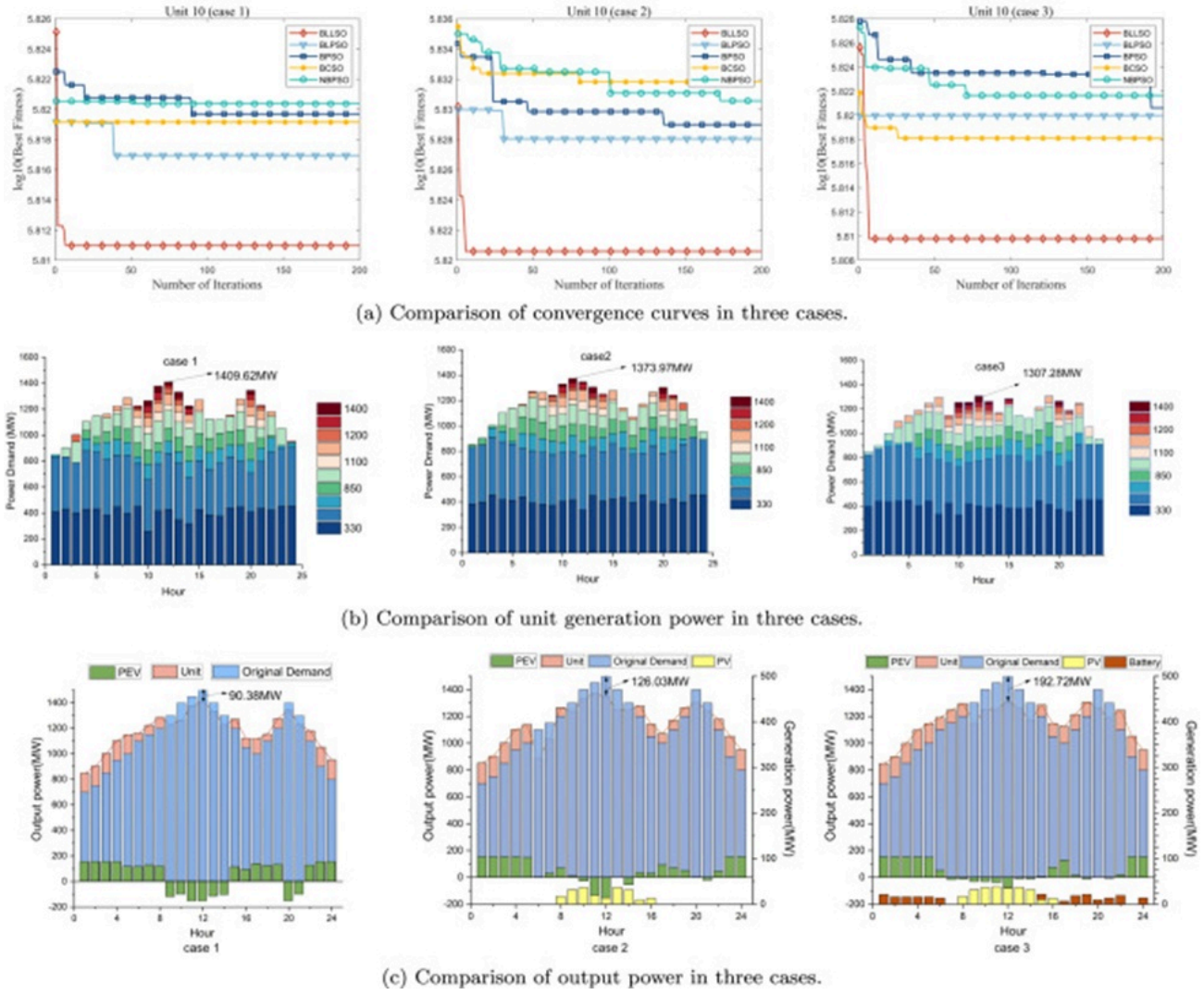


**Figure 7.** Comparison of three analytical situations in three cases.

Whichever case is considered, the tiered learning architecture underpinning BLLSO yields faster convergence and superior optimization outcomes when pitted against the rival algorithms, as attested by **Figure 7a**. The divergence between the baseline load profile and the thermal unit dispatch for the distinct cases is mapped in **Figure 7c**; in this plot, case 3 unmistakably exhibits a broader gulf separating the two traces than either case 1 or case 2. This signals that the suggested scheme can ease the demand burden weighing on conventional generation assets in the grid, while concurrently blunting the effects tied to a changing climate.

**Table 7.** The optimal results of UC integrated with PEVs and DGs.

| Hour | PEV Load (MW) | Demand (MW) | Unit10 (MW) | Unit9 (MW) | Unit8 (MW) | Unit7 (MW) | Unit6 (MW) | Unit5 (MW) | Unit4 (MW) | Unit3 (MW) | Unit2 (MW) | Unit1 (MW) |
|---|---|---|---|---|---|---|---|---|---|---|---|---|
| **1** | 153.00 | 700.00 | 0.00 | 0.00 | 0.00 | 0.00 | 0.00 | 25.00 | 0.00 | 0.00 | 422.59 | 401.18 |
| **2** | 153.00 | 750.00 | 0.00 | 0.00 | 0.00 | 0.00 | 0.00 | 25.00 | 0.00 | 0.00 | 431.85 | 442.94 |
| **3** | 153.00 | 850.00 | 0.00 | 0.00 | 0.00 | 0.00 | 0.00 | 63.55 | 0.00 | 45.64 | 451.08 | 439.50 |
| **4** | 153.00 | 950.00 | 0.00 | 0.00 | 0.00 | 52.11 | 0.00 | 130.57 | 0.00 | 20.00 | 451.45 | 445.14 |

© 2023 The Author(s). | Published by Institute of Smart Energy Systems Press

| | | | | | | | | | | | | |
|---|---|---|---|---|---|---|---|---|---|---|---|---|
| **5** | 148.73 | 1000.00 | 0.00 | 0.00 | 0.00 | 57.08 | 0.00 | 162.00 | 0.00 | 20.00 | 455.00 | 452.15 |
| **6** | 51.41 | 1100.00 | 0.00 | 0.00 | 0.00 | 36.30 | 0.00 | 154.74 | 116.78 | 91.29 | 383.61 | 407.40 |
| **7** | −16.71 | 1150.00 | 0.00 | 0.00 | 0.00 | 33.13 | 39.66 | 139.72 | 88.91 | 113.31 | 387.80 | 444.90 |
| **8** | −13.15 | 1200.00 | 0.00 | 0.00 | 0.00 | 73.34 | 55.60 | 142.38 | 115.96 | 125.74 | 446.93 | 336.74 |
| **9** | −30.36 | 1300.00 | 0.00 | 0.00 | 26.39 | 66.73 | 43.85 | 99.40 | 56.35 | 96.19 | 330.17 | 427.39 |
| **10** | −30.82 | 1400.00 | 43.92 | 37.60 | 43.38 | 63.02 | 69.40 | 101.61 | 104.20 | 65.81 | 393.50 | 331.40 |
| **11** | −37.33 | 1450.00 | 29.54 | 32.04 | 29.43 | 41.71 | 49.51 | 143.96 | 75.62 | 92.68 | 339.97 | 421.24 |
| **12** | −74.30 | 1500.00 | 52.35 | 38.27 | 35.81 | 72.94 | 51.31 | 85.30 | 98.97 | 97.23 | 370.40 | 404.70 |
| **13** | −10.55 | 1400.00 | 25.47 | 46.38 | 28.12 | 53.99 | 54.33 | 86.37 | 88.98 | 86.99 | 399.55 | 391.95 |
| **14** | −11.13 | 1300.00 | 0.00 | 0.00 | 10.00 | 60.83 | 29.03 | 90.95 | 93.03 | 69.86 | 403.79 | 412.15 |
| **15** | 5.92 | 1200.00 | 10.00 | 37.50 | 0.00 | 0.00 | 20.00 | 160.56 | 111.23 | 130.00 | 428.51 | 387.85 |
| **16** | 73.36 | 1050.00 | 0.00 | 0.00 | 0.00 | 0.00 | 0.00 | 132.45 | 77.76 | 121.38 | 430.64 | 384.47 |
| **17** | 126.30 | 1000.00 | 0.00 | 0.00 | 0.00 | 0.00 | 0.00 | 135.60 | 113.55 | 107.90 | 380.06 | 386.85 |
| **18** | 14.44 | 1100.00 | 0.00 | 0.00 | 0.00 | 25.00 | 0.00 | 162.00 | 117.01 | 96.57 | 366.10 | 447.66 |
| **19** | −10.73 | 1200.00 | 0.00 | 0.00 | 0.00 | 58.34 | 26.94 | 134.40 | 115.98 | 119.26 | 434.43 | 416.93 |
| **20** | −0.45 | 1400.00 | 31.37 | 20.55 | 46.65 | 56.37 | 48.18 | 139.69 | 89.87 | 105.55 | 349.56 | 376.49 |
| **21** | −7.10 | 1300.00 | 0.00 | 10.59 | 19.29 | 43.37 | 35.39 | 106.24 | 117.74 | 90.08 | 408.68 | 356.72 |
| **22** | 18.72 | 1100.00 | 0.00 | 0.00 | 10.00 | 85.00 | 20.00 | 127.91 | 0.00 | 94.48 | 454.34 | 455.00 |
| **23** | 153.00 | 900.00 | 0.00 | 0.00 | 0.00 | 0.00 | 80.00 | 63.00 | 0.00 | 0.00 | 455.00 | 455.00 |
| **24** | 153.00 | 800.00 | 0.00 | 0.00 | 0.00 | 0.00 | 0.00 | 40.54 | 0.00 | 0.00 | 454.74 | 455.00 |

To bring the discussion to a close, the binary LLSO formulated in this paper distinguishes itself as both competitive and computationally capable when deployed on UC problems marked by deep coupling, elevated dimensionality, and substantial intricacy. In addition, the overarching algorithmic framework provides a favorable environment for assimilating PEV charge/discharge regulation and distributed energy storage assets into the power grid, while successfully navigating intermittency challenges, reducing dependency on fossil-based fuels, and drawing the fullest possible benefit from renewable resource streams.

## The performance of LLSO algorithm for UC problems

The spotlight in this subsection falls on evaluating the prowess of the LLSO algorithm when applied to UC problem instances. Since the objective expressed in **Eq. 1** folds in both the $CO_2$ burden of PEVs and the installation expense of storage batteries, the optimization remit stretches wider than the UC problem alone. To strip away these extraneous influences and gauge the LLSO algorithm's competence with greater precision, the objective is recast into the streamlined version provided below.

© 2023 The Author(s). | Published by Institute of Smart Energy Systems Press

$$\begin{cases} F = \omega Cost + (1-\omega)\, Emission \\ Cost = min \sum_{t=1}^{T} \sum_{j=1}^{n} (F_j(P_{j,t}) z_{j,t} + SU_{j,t}(1 - z_{j,t-1}) z_{j,t}) \\ Emission = min \sum_{t=1}^{T} \sum_{j=1}^{n} F_j^{emi}(P_{j,t}) z_{j,t} \times pr_e \end{cases} \quad (23)$$

With **Eq. 23** serving as the target to be minimized, a comparative experimental campaign was mounted, squaring the newly developed BLLSO optimizer against four established PSO offshoots—BLPSO, BPSO, NBPSO [19], and BCSO [53]—to furnish evidence that BLLSO can successfully navigate the aforementioned problem landscape. The resulting economic cost figures produced by each method, together with their evolutionary convergence traces plotted for assorted unit deployment scales, are assembled in **Table 8**. Before delving into those results, two configurable parameters deserve a closer look owing to their capacity to sway optimization trajectories: the trade-off weight $\omega$ and the stratification depth L. From one vantage point, the weight embedded in the objective function orchestrates the relative emphasis placed on generation outlays versus emission penalties, so it stands to reason that disparate weight assignments might channel the search toward markedly different basins of attraction. From another perspective, the number of tiers L triggers two opposing dynamics: a relatively flat hierarchy, with few tiers, packs a larger swarm fraction into each band, which can be beneficial for sustaining diversity when higher-tier mentors are picked out, yet simultaneously pares down the assortment of tiers from which those mentors can be drawn. Conversely, a deeper tier structure widens the pool of distinct levels but shrinks the per-tier population, thereby thinning the variety among the elite particles that serve as update templates.

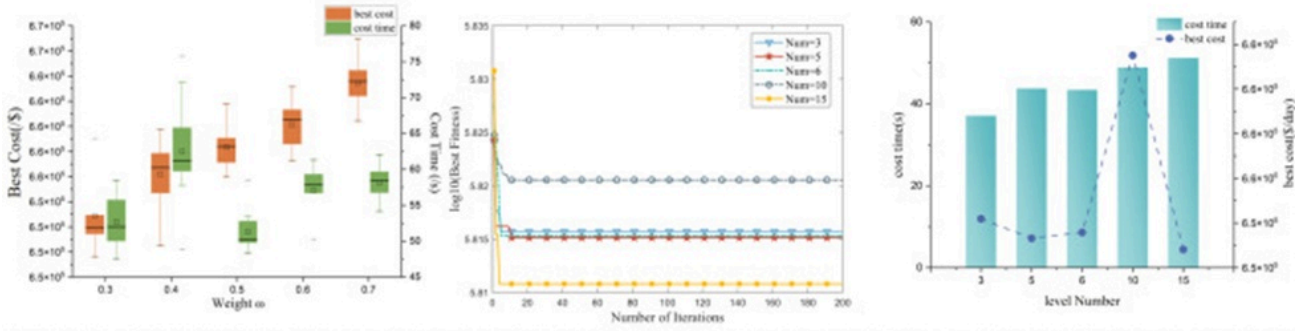


(a) The influence of different levels on the optimization results (b) The influence of different levels on convergence results (c) Compare results of different weights for the objective function

**Figure 8.** Simulation results of different level numbers for the proposed LLSO.

**Table 8.** The comparison of economic costs between BLLSO and other algorithms ($/day).

| Units \ Methods | BLJSO | BPSO | BLPSO | BCSO | NBPSO |
|---|---|---|---|---|---|
| 10 | 641151.03 | 660232.42 | 656059.77 | 659405.81 | 661257.79 |
| 20 | 1298683.07 | 1361712.85 | 1365531.02 | 1350198.56 | 1366159.31 |
| 40 | 2932930.70 | 3033901.32 | 3036362.36 | 3027874.59 | 3045861.33 |
| 60 | 5031276.71 | 5081598.26 | 5120236.23 | 5176234.85 | 5141295.51 |
| 80 | 7658985.91 | 7735412.70 | 7764308.78 | 7770574.64 | 7739865.17 |
| 100 | 10532931.32 | 10661547.12 | 10701986.46 | 10694520.02 | 10753241.4 |

Keeping this dual-edged dynamic in view, it is plausible that the tier count could cut both ways during the search progression. The simulated outcomes across a sweep of weight magnitudes and tier configurations, applied to the 10-unit

© 2023 The Author(s). | Published by Institute of Smart Energy Systems Press

benchmark, are plotted in **Figure 8**; these plots show that alternative tier designs indeed push the optimizer toward divergent end states. As **Figure 8a** makes plain, elevating the weight coefficient drives the ultimate economic value upward, although the accompanying computational toll does not follow a uniform trajectory. The computational expenditure gap separating the weight settings of 0.3 and 0.5 proves narrower than that seen between most other weight pairs; even so, adopting a weight of 0.5 inflates the final economic cost relative to what is achieved at 0.3. Hence, pinning the weight at 0.3 strikes an acceptable middle ground, balancing economic returns against computational load. When the tier count sits at L = 10, **Figures 8b and 8c** reveal that both the optimization quality attained and the rate at which convergence unfolds are inferior to configurations where L stays below the 10 mark. By contrast, deepening the hierarchy to 15 tiers brings about a clear upswing in both solution fidelity and convergence momentum. Determining a sensible tier tally, therefore, exerts a tangible influence on reconciling the tension between wide-ranging exploration and focused exploitation.

Shifting focus to **Table 8**, the economic costs distilled by each competing algorithm for the UC formulation are placed side by side, spanning unit complement sizes of 10, 20, 40, 60, 80, and 100. The story told by the table is unambiguous: BLLSO unfailingly undercuts all rival algorithms on economic cost, without exception across every fleet scale tested. Moreover, the problem's dimensionality scales directly with the unit headcount; for a 10-unit system, the dimensionality equals 10 (units) × 24 (hours) = 240. The slimmest improvement margin BLLSO opens up over its nearest competitor amounts to 14908.74 $/day, while the largest advantage balloons to a striking 220310.1 $/day when the unit count reaches the 100 mark. These numbers attest to BLLSO's latent strength and viability for confronting large-scale, high-dimensional UC formulations. **Figure 9** reinforces this narrative, showing that BLLSO handily outclasses the comparison group on both the swiftness of convergence and the caliber of the end-point solution. This dominance can be credited to BLLSO's layered learning paradigm, which injects greater heterogeneity into the population and thus lowers the odds of premature stagnation or settling on suboptimal plateaus. Even when the generating fleet is expanded to 100 units, BLLSO preserves its lead in both the speed with which it converges and the quality of the solutions it uncovers. Taken as a whole, the evidence shows that LLSO not only achieves a well-calibrated equilibrium between exploratory and exploitative search modes but also proves itself well-adapted to the demands of large-scale optimization settings.

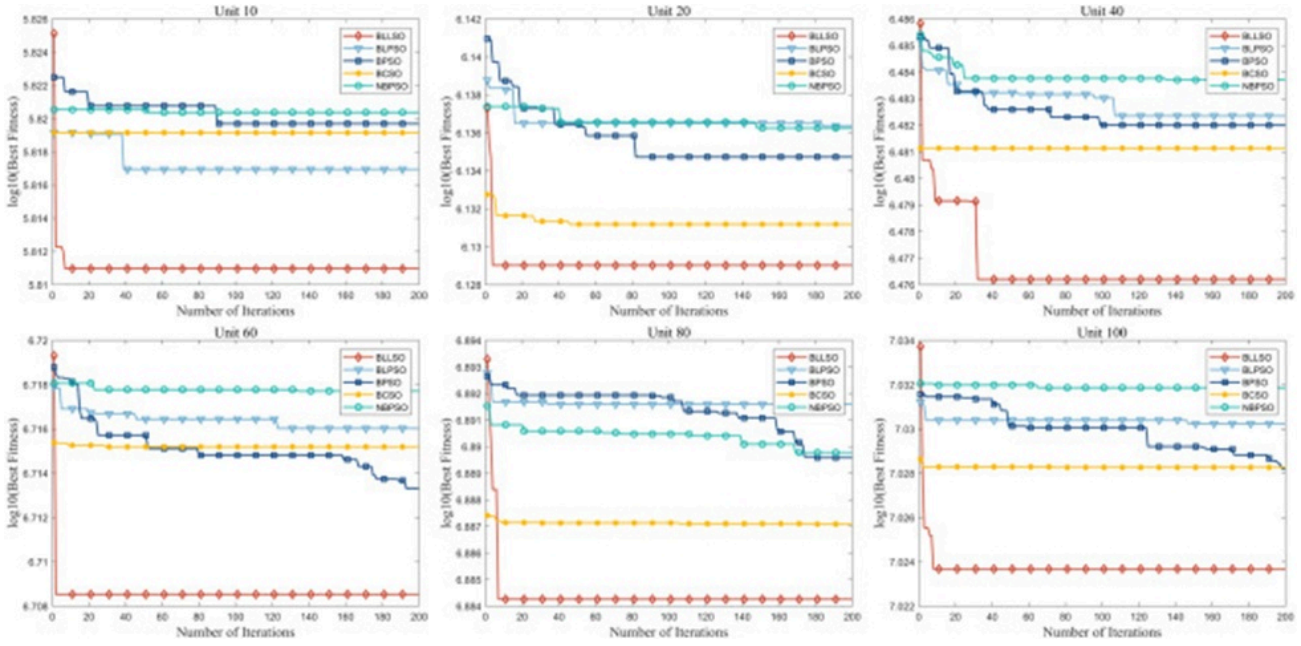


**Figure 9.** Convergence curves of different algorithms with different unit numbers.

# Conclusion

© 2023 The Author(s). | Published by Institute of Smart Energy Systems Press

Weaving plug-in electric vehicles, photovoltaic generation, and battery-based energy storage into the fabric of the power system unlocks a host of advantages—spanning grid steadiness, peak load containment, renewable resource accommodation, and smarter infrastructure utilization—while giving rise to a sizable optimization undertaking. This study advances a multi-energy synergy system scheduling construct to give structure to the problem. Building on this, a large-scale binary level-based learning swarm optimizer is proposed to govern generating units, explicitly accommodating the binary on/off nature of unit commitment decisions and seeking to jointly minimize fossil-fuel-related expenditures and carbon emission penalties via the objective function. Within this architectural frame, the binary level-based learning swarm optimization routine is deployed to refine the effects of PEV charge/discharge orchestration, stationary battery storage, and photovoltaic infeed on grid performance.

To gauge the practical viability and indispensability of the proposed blueprint, three distinct operational vignettes are explored, and the financial benefits they confer on the grid are scrutinized. The experimental evidence confirms that the suggested algorithmic approach can trim costs by upwards of 3.3%, underscoring a formidable competitive aptitude for untangling intricate, high-dimensional energy system problems. It follows logically that the disciplined charging and discharging of plug-in electric vehicles, in concert with distributed energy storage deployment, will occupy a central role in the power grids of the coming era; their low-carbon profile and renewable pedigree stand to deliver tangible economic returns while simultaneously spurring the broader adoption of renewable energy and accelerating the transition toward multi-energy synergy systems.

## Acknowledgements

None

## Conflict of interest

None

## Financial support

This research is financially supported by National Natural Science Foundation of China under grants 52077213 and 62003332, and Youth Innovation Promotion Association CAS 2021358, and Shenzhen Science and Technology Research and Development Fund JCYJ20200109114839874, and NSFC-FDCT under its Joint Scientific Research Project Fund (Grant No. 0051/2022/AFJ), China & Macau.

## Ethics statement

None

Received: 18 Jun 2022 Revised: 26 Aug 2022 Accepted: 12 Sep 2022
Published online: 15 November 2023

### Rights and permissions

**Open Access** The author(s) retain copyright. This article is licensed under the Creative Commons Attribution-NonCommercial-ShareAlike 4.0 International License. It may be shared and adapted for non-commercial purposes with appropriate attribution, an indication of changes, and

distribution of adaptations under the same license. Third-party material may be subject to separate terms identified in its credit line. View the license at https://creativecommons.org/licenses/by-nc-sa/4.0/.

# References

1. Liu Z, Sun Y, Xing C, Liu J, He Y, Zhou Y, et al. Artificial intelligence powered large-scale renewable integrations in multi-energy systems for carbon neutrality transition: Challenges and future perspectives. Energy AI. 2022;100195.

2. Yang S, Gao HO, You F. Integrated optimization in operations control and systems design for carbon emission reduction in building electrification with distributed energy resources. Adv Appl Energy. 2023;100144.

3. Sharma H, Marinovici L, Adetola V, Schaef HT. Data-driven modeling of power generation for a coal power plant under cycling. Energy AI. 2023;11:100214.

4. Yang W, Guo J, Vartosh A. Optimal economic-emission planning of multi-energy systems integrated electric vehicles with modified group search optimization. Appl Energy. 2022;311:118634.

5. Turk A, Wu Q, Zhang M, Østergaard J. Day-ahead stochastic scheduling of integrated multi-energy system for flexibility synergy and uncertainty balancing. Energy. 2020;196:117130.

6. Liu X, Yan Z, Wu J. Optimal coordinated operation of a multi-energy community considering interactions between energy storage and conversion devices. Appl Energy. 2019;248:256-73.

7. Shahbakhsh A, Nieße A. Modeling multimodal energy systems. Automatisierungstechnik. 2019;67(11):893-903.

8. Yang Z, Li K, Guo Y, Feng S, Niu Q, Xue Y, et al. A binary symmetric based hybrid meta-heuristic method for solving mixed integer unit commitment problem integrating with significant plug-in electric vehicles. Energy. 2019;170:889-905.

9. Zou W, Sun Y, Gao D-c, Zhang X, Liu J. A review on integration of surging plug-in electric vehicles charging in energy-flexible buildings: Impacts analysis, collaborative management technologies, and future perspective. Appl Energy. 2023;331:120393.

10. Zhang H, Moura SJ, Hu Z, Qi W, Song Y. Joint PEV charging network and distributed PV generation planning based on accelerated generalized benders decomposition. IEEE Trans Transp Electr. 2018;4(3):789-803.

11. Lander L, Kallitsis E, Hales A, Edge JS, Korre A, Offer G. Cost and carbon footprint reduction of electric vehicle lithium-ion batteries through efficient thermal management. Appl Energy. 2021;289:116737.

12. Lagos DT, Hatziargyriou ND. Data-driven frequency dynamic unit commitment for island systems with high RES penetration. IEEE Trans Power Syst. 2021;36(5):4699-711.

13. Kermani M, Shirdare E, Parise G, Bongiorno M, Martirano L. A comprehensive technoeconomic solution for demand control in ports: Energy storage systems integration. IEEE Trans Ind Appl. 2022;58(2):1592-601.

14. Zsiborács H, Pintér G, Vincze A, Baranyai NH, Mayer MJ. The reliability of photovoltaic power generation scheduling in seventeen European countries. Energy Convers Manage. 2022;260:115641.

15. Furukakoi M, Adewuyi OB, Matayoshi H, Howlader AM, Senjyu T. Multi objective unit commitment with voltage stability and PV uncertainty. Appl Energy. 2018;228:618-23.

16. Saber AY, Venayagamoorthy GK. Plug-in vehicles and renewable energy sources for cost and emission reductions. IEEE Trans Ind Electron. 2011;58(4):1229-38.

© 2023 The Author(s). | Published by Institute of Smart Energy Systems Press

17. Joos M, Staffell I. Short-term integration costs of variable renewable energy: Wind curtailment and balancing in Britain and Germany. Renew Sustain Energy Rev. 2018;86:45-65.

18. Yang Z, Yang F, Min H, Tian H, Hu W, Liu J, et al. Energy management programming to reduce distribution network operating costs in the presence of electric vehicles and renewable energy sources. Energy. 2023;263:125695.

19. Yang Z, Li K, Niu Q, Xue Y. A novel parallel-series hybrid meta-heuristic method for solving a hybrid unit commitment problem. Knowl-Based Syst. 2017;134:13-30.

20. Boretti A. Integration of solar thermal and photovoltaic, wind, and battery energy storage through AI in NEOM city. Energy AI. 2021;3:100038.

21. Yildiz B, Stringer N, Klymenko T, Samhan MS, Abramowitz G, Bruce A, et al. Real-world data analysis of distributed PV and battery energy storage system curtailment in low voltage networks. Renew Sustain Energy Rev. 2023;186:113696.

22. Zeraati M, Golshan MEH, Guerrero JM. Distributed control of battery energy storage systems for voltage regulation in distribution networks with high PV penetration. IEEE Trans Smart Grid. 2016;9(4):3582-93.

23. Fleer J, Stenzel P. Impact analysis of different operation strategies for battery energy storage systems providing primary control reserve. J Energy Storage. 2016;8:320-38.

24. Guzmán-Feria JS, Castro LM, Tovar-Hernández J, González-Cabrera N, Gutiérrez-Alcaraz G. Unit commitment for multi-terminal VSC-connected AC systems including BESS facilities with energy time-shifting strategy. Int J Electr Power Energy Syst. 2022;134:107367.

25. Huang P, Sun Y, Lovati M, Zhang X. Solar-photovoltaic-power-sharing-based design optimization of distributed energy storage systems for performance improvements. Energy. 2021;222:119931.

26. Nishanthy J, Raja SC, Nesamalar JJD. Feasibility analysis of solar PV system in presence of EV charging with transactive energy management for a community-based residential system. Energy Convers Manage. 2023;288:117125.

27. Li Y, Wang P, Gooi HB, Ye J, Wu L. Multi-objective optimal dispatch of microgrid under uncertainties via interval optimization. IEEE Trans Smart Grid. 2019;10(2):2046-58.

28. Neri A, Butturi MA, Lolli F, Gamberini R. Inter-firm exchanges, distributed renewable energy generation, and battery energy storage system integration via microgrids for energy symbiosis. J Clean Prod. 2023;414:137529.

29. Su W, Chow M-Y. Computational intelligence-based energy management for a large-scale PHEV/PEV enabled municipal parking deck. Appl Energy. 2012;96:171-82.

30. Borozan S, Giannelos S, Strbac G. Strategic network expansion planning with electric vehicle smart charging concepts as investment options. Adv Appl Energy. 2022;5:100077.

31. Naderipour A, Kamyab H, Klemeš JJ, Ebrahimi R, Chelliapan S, Nowdeh SA, et al. Optimal design of hybrid grid-connected photovoltaic/wind/battery sustainable energy system improving reliability, cost and emission. Energy. 2022;257:124679.

32. Gomes I, Melicio R, Mendes V. A novel microgrid support management system based on stochastic mixed-integer linear programming. Energy. 2021;223:120030.

33. Colonetti B, Finardi E, Brito S, Zavala V. Parallel dual dynamic integer programming for large-scale hydrothermal unit-commitment. IEEE Trans Power Syst. 2022;38(3):2926-38.

34. Jiang Q, Zhou B, Zhang M. Parallel augment Lagrangian relaxation method for transient stability constrained unit commitment. IEEE Trans Power Syst. 2013;28(2):1140-8.

© 2023 The Author(s). | Published by Institute of Smart Energy Systems Press

35. Feng F, Zhang P, Bragin MA, Zhou Y. Novel resolution of unit commitment problems through quantum surrogate Lagrangian relaxation. IEEE Trans Power Syst. 2022.

36. Arroyo JM, Conejo AJ. A parallel repair genetic algorithm to solve the unit commitment problem. IEEE Trans Power Syst. 2002;17(4):1216-24.

37. Trivedi A, Srinivasan D, Biswas S, Reindl T. A genetic algorithm–differential evolution based hybrid framework: case study on unit commitment scheduling problem. Inform Sci. 2016;354:275-300.

38. Simon SP, Padhy NP, Anand RS. An ant colony system approach for unit commitment problem. Int J Electr Power Energy Syst. 2006;28(5):315-23.

39. Ting T, Rao M, Loo C. A novel approach for unit commitment problem via an effective hybrid particle swarm optimization. IEEE Trans Power Syst. 2006;21(1):411-8.

40. Hussein BM, Jaber AS. Unit commitment based on modified firefly algorithm. Meas Control. 2020;53(3-4):320-7.

41. Roy PK, Sarkar R. Solution of unit commitment problem using quasi-oppositional teaching learning based algorithm. Int J Electr Power Energy Syst. 2014;60:96-106.

42. Yuan X, Su A, Nie H, Yuan Y, Wang L. Application of enhanced discrete differential evolution approach to unit commitment problem. Energy Convers Manage. 2009;50(9):2449-56.

43. Hussien AG, Hassanien AE, Houssein EH, Amin M, Azar AT. New binary whale optimization algorithm for discrete optimization problems. Eng Optim. 2020;52(6):945-59.

44. Pan J-S, Hu P, Chu S-C. Binary fish migration optimization for solving unit commitment. Energy. 2021;226:120329.

45. Kashan MH, Nahavandi N, Kashan AH. DisABC: a new artificial bee colony algorithm for binary optimization. Appl Soft Comput. 2012;12(1):342-52.

46. Lau T, Chung C, Wong K, Chung T, Ho SL. Quantum-inspired evolutionary algorithm approach for unit commitment. IEEE Trans Power Syst. 2009;24(3):1503-12.

47. Rizk-Allah RM. A quantum-based sine cosine algorithm for solving general systems of nonlinear equations. Artif Intell Rev. 2021;54(5):3939-90.

48. Wang F, Zhang H, Zhou A. A particle swarm optimization algorithm for mixed-variable optimization problems. Swarm Evol Comput. 2021;60:100808.

49. Cheng R, Sun C, Jin Y. A multi-swarm evolutionary framework based on a feedback mechanism. In: 2013 IEEE congress on evolutionary computation. IEEE; 2013. p. 718-24.

50. Wang X, Henshaw P, Ting DS-K. Exergoeconomic analysis for a thermoelectric generator using mutation particle swarm optimization (m-PSO). Appl Energy. 2021;294:116952.

51. Cheng R, Jin Y. A social learning particle swarm optimization algorithm for scalable optimization. Inform Sci. 2015;291(C):43-60.

52. Wang X, Zhang K, Wang J, Jin Y. An enhanced competitive swarm optimizer with strongly convex sparse operator for large-scale multiobjective optimization. IEEE Trans Evol Comput. 2021;26(5):859-71.

53. Wang Y, Yang Z, Mourshed M, Guo Y, Niu Q, Zhu X. Demand side management of plug-in electric vehicles and coordinated unit commitment: A novel parallel competitive swarm optimization method. Energy Convers Manage. 2019;196:935-49.

© 2023 The Author(s). | Published by Institute of Smart Energy Systems Press

54. Zhu X, Zhao S, Yang Z, Zhang N, Xu X. A parallel meta-heuristic method for solving large scale unit commitment considering the integration of new energy sectors. Energy. 2022;238:121829.

55. Feng L, Shang Q, Hou Y, Tan KC, Ong Y-S. Multispace evolutionary search for large-scale optimization with applications to recommender systems. IEEE Trans Artif Intell. 2022;4(1):107-20.

56. Li X, Lu S, Li Z, Wang Y, Zhu L. Modeling and optimization of bioethanol production planning under hybrid uncertainty: A heuristic multi-stage stochastic programming approach. Energy. 2022;245:123285.

57. Yang Q, Chen W-N, Da Deng J, Li Y, Gu T, Zhang J. A level-based learning swarm optimizer for large-scale optimization. IEEE Trans Evol Comput. 2017;22(4):578-94.

58. Zhang N, Hu Z, Dai D, Dang S, Yao M, Zhou Y. Unit commitment model in smart grid environment considering carbon emissions trading. IEEE Trans Smart Grid. 2015;7(1):420-7.

59. Lund H, Kempton W. Integration of renewable energy into the transport and electricity sectors through V2G. Energy Policy. 2008;36(9):3578-87.

60. Gaing Z-L. Discrete particle swarm optimization algorithm for unit commitment. In: 2003 IEEE power engineering society general meeting. vol. 1. IEEE; 2003. p. 418-24.

61. Cheng R, Jin Y. A social learning particle swarm optimization algorithm for scalable optimization. Inform Sci. 2015;291:43-60. (Duplicate of #51, omitted)

62. Cheng R, Jin Y. A competitive swarm optimizer for large scale optimization. IEEE Trans Cybern. 2014;45(2):191-204.

63. Kazarlis SA, Bakirtzis AG, Petridis V. A genetic algorithm solution to the unit commitment problem. IEEE Trans Power Syst. 1996;11(1):83-92.

64. Zhao S, Li K, Yang Z, Xu X, Zhang N. A new power system active rescheduling method considering the dispatchable plug-in electric vehicles and intermittent renewable energies. Appl Energy. 2022;314:118715.

65. Xing C, Li K, Su J. Thermal constrained energy optimization of railway co-phase systems with ESS integration-an FRA-pruned DQN approach. IEEE Trans Transp Electr. 2022.

66. Quan H, Srinivasan D, Khambadkone AM, Khosravi A. A computational framework for uncertainty integration in stochastic unit commitment with intermittent renewable energy sources. Appl Energy. 2015;152:71-82.

© 2023 The Author(s). | Published by Institute of Smart Energy Systems Press